이학박사 학위논문

폐암세포에서 Hedgehog signaling 에 의한 $KRAS^{G12C}$ 억제제에 대한 내성획득 기전

Hedgehog signaling is involved in acquired resistance against $KRAS^{G12C}$ inhibitors in lung cancer cells

울산대학교 대학원
생명과학과
이채영

폐암세포에서 Hedgehog signaling 에 의한 $KRAS^{G12C}$ 억제제에 대한 내성획득 기전

지 도 교 수 박 정 우

이 논문을 이학박사 학위 논문으로 제출함

2024 년 2 월

울산대학교 대학원
생명과학과
이채영

이채영의 이학박사 학위 논문을 인준함

심 사 위 원 장	정 헌 택	
심 사 위 원	박 정 우	
심 사 위 원	권 혁 남	
심 사 위 원	소 홍 섭	
심 사 위 원	이 정 진	

울산대학교 대학원

2024 년 2 월

Hedgehog signaling is involved in acquired resistance against $KRAS^{G12C}$ inhibitors in lung cancer cells

Supervisor: Jung-Woo Park, Ph.D

A Dissertation

Submitted to
the Graduate School of the University of Ulsan
In partial Fulfillment of the Requirements
For the Degree of

Doctor of Philosophy

by

Chaeyoung Lee

Department of Biological Science
Graduate School
University of Ulsan, Korea
February, 2024

CONTENTS

Hedgehog signaling is involved in acquired resistance against $KRAS^{G12C}$ inhibitors in lung cancer cells

I. Abstract ---------- 1

II. Introduction ---------- 2

III. Materials and Methods ---------- 5

Cell culture and reagents

RAS-GTP pull-down assay

SDS-PAGE and immunoblotting

Quantitative and semiquantitative real-time PCR

Cell cycle analysis

Immunostaining and quantification of ciliated cells

RNA preparation and RNA-seq

Clonogenic assay

Chromatin immunoprecipitation assay

Plasmids, small interfering RNAs, transfections, and luciferase assay

Statistical analysis

IV. Results ---------- 11

$KRAS^{G12C}$-mutant cancer cells initially respond to $KRAS^{G12C}$ inhibitors but rapidly re-express $KRAS^{G12C}$ and reactivate ERK

RNA-seq analysis reveals the induction of Hh pathway in $KRAS^{G12C}$-mutant cancer cells after $KRAS^{G12C}$ inhibitor treatment

$KRAS^{G12C}$ inhibitors enhance the Hh signal and primary cilia in cancer cells

Downregulation of AURKA mediates the induction of Hh signaling and re-expression of KRAS after treatment with a $KRAS^{G12C}$ inhibitor

Inhibition of Hh signals blocks re-expression of KRAS and reactivation of ERK in $KRAS^{G12C}$ inhibitor–treated cancer cells

GLI-1 is responsible for reactivation of KRAS induced by $KRAS^{G12C}$ inhibitor in cancer cells

V. Figures and Table ---------- 18

VI. Discussion ---------- 54

VII. References ---------- 58

I. Abstract

Although $KRAS^{G12C}$ inhibitors have shown promising activity in lung adenocarcinomas harboring $KRAS^{G12C}$, acquired resistance to these therapies eventually occurs in most patients. Re-expression of KRAS is thought to be one of the main causes of acquired resistance. However, the mechanism through which cancer cells re-express KRAS is not fully understood. Here, the present study reports that the Hedgehog signal is induced by $KRAS^{G12C}$ inhibitors and mediates KRAS re-expression in cancer cells treated with a $KRAS^{G12C}$ inhibitor. Further, $KRAS^{G12C}$ inhibitors induced the formation of primary cilia and activated the Hedgehog-GLI-1 pathway. GLI-1 binds to the KRAS promoter region, enhancing KRAS promoter activity and KRAS expression. Inhibition of GLI using siRNA or the smoothened (Smo) inhibitor suppressed re-expression of KRAS in cells treated with a $KRAS^{G12C}$ inhibitor. In addition, the $KRAS^{G12C}$ inhibitors decreased Aurora kinase A (AURKA) levels in cancer cells, and inhibition of AURKA using siRNA or inhibitors led to increased expression levels of GLI-1 and KRAS even in the absence of KRAS inhibitor. Ectopic expression of AURKA attenuated the effect of $KRAS^{G12C}$ inhibitors on the expression of GLI-1 and re-expression of KRAS. Together, these findings demonstrate the important role of AURKA, primary cilia, and Hedgehog signals in the re-expression of KRAS and therefore the induction of acquired resistance to $KRAS^{G12C}$ inhibitors, and provide a rationale for targeting Hedgehog signaling to overcome acquired resistance to $KRAS^{G12C}$ inhibitors.

Running title: Hh signaling induces acquired resistance against $KRAS^{G12C}$ inhibitors

II. Introduction

The KRAS protein is a GTPase that functions as a molecular switch that cycles between active GTP-bound and inactive GDP-bound states (1). The binding of GTP to KRAS promotes the binding of effectors that trigger signal transduction pathways, including the RAF-MEK-ERK (MAPK) pathway (2, 3). Activating mutations in the *KRAS* gene are a hallmark of cancer (4) and the $KRAS^{G12C}$ protein mutation is one of the most common activating alterations in lung adenocarcinoma (5). $KRAS^{G12C}$ mutations occur in approximately 13% of lung adenocarcinomas and 3% of colorectal adenocarcinomas, and less commonly in cancers of the uterus, pancreas, breast, bladder, cervix, and ovaries (6, 7). A $KRAS^{G12C}$ mutation results in an increase of GTP-bound activated KRAS (8) and activates downstream signaling pathways that allow cells to grow uncontrollably (9).

Due to the intrinsic characteristics of KRAS proteins, KRAS has been considered an undruggable target. KRAS proteins have relatively smooth surfaces, no obvious deep hydrophobic pockets to which drugs can bind (10), and high affinity for GTPs, which make it difficult to interfere with GTP binding using GTP analogs (11). However, after discovering allosteric inhibitors that can bind cysteine 12 residues within the switch II region of the $KRAS^{G12C}$ mutant, thereby locking the protein in its inactive GDP-bound state (12), several $KRAS^{G12C}$ inhibitors have been identified that bind covalently to the GDP-bound form of the $KRAS^{G12C}$ protein, preventing oncogenic signaling and causing tumor regression in preclinical models (8, 12, 13). In early-phase clinical trials, two small-molecule $KRAS^{G12C}$ inhibitors, adagrasib (MRTX849) and sotorasib (AMG 510), have shown promising results against non–small cell lung cancer and more modest efficacy against colorectal cancer (13, 14). Despite the clinical benefits observed for many patients treated with $KRAS^{G12C}$ inhibitors, most patients eventually acquire resistance to single-agent therapy. Acquired resistance to $KRAS^{G12C}$

inhibitors can be caused by various mechanisms (15), including genetic changes such as secondary mutations in $KRAS^{G12C}$ that interfere with the binding of covalent inhibitors to cysteine 12 residues, and other mutations related to the reactivation of the RAS-RAF-MEK-ERK signaling pathway (16, 17). In addition to genetic changes, acquired resistance can be induced by synthesizing new $KRAS^{G12C}$ proteins and reactivating downstream signaling (18). Similarly, reactivation of the MAPK pathway without new mutations in KRAS or its downstream mediators has been reported in $KRAS^{G12C}$ lung adenocarcinomas resistant to the $KRAS^{G12C}$ inhibitor AMG 510 (19). Further analysis has revealed that epidermal growth factor receptor or Aurora kinase A (AURKA) signals can maintain newly expressed $KRAS^{G12C}$ proteins in an active GTP-bound form, thereby evading treatment by $KRAS^{G12C}$ inhibitors (18). However, another study suggests that wild-type RAS activation mediated by multiple-*receptor tyrosine kinases (*RTKs), rather than a single RTK, is responsible for acquired resistance to the $KRAS^{G12C}$ inhibitors ARS-1620 and sotorasib in various cancer cell lines (20). Ultimately, an improved understanding of the biological basis of drug resistance will provide more opportunities to optimize $KRAS^{G12C}$-inhibitor regimens and new combinations.

Hedgehog (Hh) signaling plays a pivotal role in regulating a number of cell-fate and self-renewal processes during development and tissue homeostasis (21). Vertebrate Hh signaling is transduced by the primary cilium, a cellular antenna that projects from the surface of most cells (22, 23). The seven transmembrane domain-containing protein known as smoothened (Smo) serves as a key player in Hh signaling. In the absence of Hh ligands, the Hh receptors patched 1 (PTCH1) and PTCH2 at the cilium inhibit Smo, keeping the pathway in its off state (24). When Hh ligands bind to their receptor PTCHs at the cilium, inhibition of Smo ceases and Smo accumulates at the cilium, where it activates the downstream pathway (25). Upon Hh pathway activation, glioma-associated oncogene 1 (GLI-1) transcription factors are activated and

regulate target gene expression by direct association with a specific consensus sequence in the promoter region of the target genes (26).

This study identified that, consistent with a previous report (18), mutant $KRAS^{G12C}$ cancer cells initially responded to $KRAS^{G12C}$ inhibitors but then rapidly re-expressed $KRAS^{G12C}$ and re-activated its downstream extracellular signal–regulated kinase (ERK). These changes are associated with upregulation of the Hh signal, cilia frequency, and cilia length. Inhibition of the Hh signaling pathway blocks re-expression of $KRAS^{G12C}$, reactivation of ERK, and resumption of cell proliferation after treatment with a $KRAS^{G12C}$ inhibitor. These results suggest that upregulation of the Hh pathway plays a critical role in inducing acquired resistance of mutant $KRAS^{G12C}$ cancer cells against $KRAS^{G12C}$ inhibitors, providing a rationale for targeting the Hh pathway as a strategy to overcome acquired resistance to $KRAS^{G12C}$ inhibitors.

III. Materials and Methods

Cell culture and reagents

Human non–small cell lung carcinoma H358 (CRL-5807, KCLB 25807) and H23 (CRL-5800, KCLB 90023) cell lines harboring the $KRAS^{G12C}$ mutation were purchased from the Korean Cell Line Bank (KCLB, Seoul, Korea). Cells were maintained in RPMI-1640 medium supplemented with 10% fetal bovine serum, penicillin, streptomycin and 2 mM L-glutamine. The $KRAS^{G12C}$ inhibitors ARS-1620 (S8707) and AMG 510 (S8830), Smo inhibitor sonidegib (S2151), and AURKA inhibitor Tozasertib (S1048) were purchased from Selleck Chemicals (Selleck Chemicals LLC, Houston, TX, USA) and administered at 10 μM, or as otherwise specified, in culture.

RAS-GTP pull-down assay

Determination of GTP-bound KRAS levels was performed using the Active Ras Pull-Down and Detection Kit (Thermo Fisher Scientific, 16117) according to the manufacturer's instruction. Briefly, whole-cell lysates were incubated with recombinant glutathione *S*-transferase (GST)-tagged Raf1 RBD protein, followed by Glutathione-agarose beads, to isolate the bound KRAS-GTP. The samples were then subjected to western blotting with an anti-KRAS antibody (Sigma, WH0003845M1). Total KRAS was determined by blot analyses with an anti-KRAS antibody (Sigma, WH0003845M1) using the whole-cell lysate.

SDS-PAGE and immunoblotting

Cells were lysed in a RIPA lysis and extraction buffer (Thermo Fisher Scientific, 78501) with protease (Roche, 04693132001) and phosphatase inhibitors (Roche, 04906837001) on ice. Samples were separated by sodium dodecyl sulfate–polyacrylamide gel electrophoresis (SDS-

PAGE) followed by transfer to nitrocellulose membranes (GE, 10600001). Membranes were probed with primary antibodies against mouse anti-ERK (Cell Signaling, 9107), rabbit anti-phospho-Erk (Cell Signaling, 9101), rabbit anti-IFT88 (Proteintech, 13967-1-AP), mouse anti-ARL6 (Proteintech, 12676-1-AP), rabbit anti-GLI-1 (Cell Signaling, 2553), rabbit anti-AURKA (Cell Signaling, 4718), and mouse anti-β-actin (Sigma, A5441). Immunoreactivity bands were detected using a Pierce electrochemiluminescence western blotting substrate (Thermo Fisher Scientific, 34850).

Quantitative and semiquantitative real-time PCR

Total RNA from cells was extracted using a TRIzol reagent (Invitrogen, 15596018). Synthesis of cDNA used 2 μg of total RNA, oligo-dT, and Superscript II reverse transcriptase (Invitrogen, 18064022). Templates for quantitative real-time polymerase chain reaction (qRT-PCR) amplification of gene specific primers are listed in Table 1. All qRT-PCR analyses included real-time monitoring of the increase in fluorescence of SYBR Green dye (Abm, G891, Canada) using a StepOne real-time PCR system (Applied Biosystems). Semiquantitative RT-PCR was performed using a Taq polymerase (Solgent, STD02-M50h, Daejeon, Korea).

Cell cycle analysis

The effect of the $KRAS^{G12C}$ inhibitor ARS-1620 on cell cycle distribution was examined by propidium iodide staining followed by FACS Scan Flow cytometry analysis. Briefly, H358 cells at 50% confluency were treated with 10 μM ARS-1620 for the indicated times. Cells were collected and fixed in ice-cold 70% ethanol at 4 °C for 24 h. After washing with phosphate-buffered solution (PBS), cells were stained by incubating them with a freshly made PBS solution containing 20 μg/mL propidium iodide (Thermo Fisher Scientific, P3566) and 0.2

mg/mL ribonuclease A (Thermo Fisher Scientific, EN0531) at 37 °C for 30 min in the dark. Cell cycle distribution in the prepared cells was estimated by measuring the cell's DNA content according to the standard procedures using FACS Canto II (Beckton Dickinson).

Immunostaining and quantification of ciliated cells

Cells were treated with a combination of 10 μM ARS-1620 and 10 μM Sonidegib for 72 h and fixed with 4% paraformaldehyde and 0.3% (v/v) Triton X-100 in PBS for 10 min. After blocking the cells with 5% bovine serum albumin (BSA) in PBS, the cells were incubated overnight at 4 °C with primary antibodies against acetylated α-tubulin (T7451, Sigma-Aldrich) and a small GTPase Arl13B enriched in primary cilia (27) (17711-1-AP, Proteintech) in 1% BSA. After washing, the cells were incubated with Alexa Fluor-conjugated secondary antibodies (Life Technologies) at room temperature for 1 h. Nuclei were detected with 1 μg/mL 4′,6-diamidino-2-phenylindole (Sigma-Aldrich). The stained cells were examined using an Olympus 1000/1200 laser-scanning confocal system. Cilia were counted in approximately 150 cells under each experimental condition. The percentage of ciliated cells was calculated as (total number of cilia)/(total number of DAPI-labeled nucleus at each image) × 100. Cilia lengths were measured using the Free-hand Line Selection Tool of Cell Sense Standards software (Olympus Europa Holding GmbH, Hamburg, Germany) and average cilium lengths were calculated. Data analysis was performed in GraphPad Prism 8 (GraphPad Software, San Diego, CA).

RNA preparation and RNA-seq

The performed RNA-seq analysis on total RNA samples (RIN > 8.5) collected from H358 cells at 0, 12, and 48 h after treatment with 10 μM ARS-1620 or 10 μM Sonidegib. Residual DNA

from each sample was removed using the RNeasy MinElute Cleanup Kit (Qiagen, Hilden, Germany). Libraries of cDNA were prepared with 1.0 μg of total RNA using the TrueSeq RNA Library Preparation Kit (Illumina, San Diego, CA, USA) following the manufacturer's recommendations, followed by paired-end sequencing (2 × 100 bp) using the HiSeq1500 platform (Illumina, San Diego, CA, USA). Amplification of cDNA was carried out according to the RNA-seq protocol provided by Illumina and sequenced using an Illumina HiSeq 2500 system to obtain 150-bp paired-end reads. Sequencing depth for each sample was > 20 million reads. RNA-seq reads were mapped to the human genome GRCh38/hg38 using STAR 2.7.9a (28). The featureCounts function of the Rsubread package was used to generate count tables. The DESeq2 package (29) was used to generate a DEG list object from feature counts. Genes with a false discovery rate (adjusted P value < 0.05 and log2 fold change > 1.5) were selected as DEGs. Normalized read counts were used for hierarchical clustering by hclust in R. The count table generated by featureCounts was subjected to further GSEA (Java, GSEA Desktop Application version 3.0; http://software.broadinstitute.org/gsea/downloads.jsp). Positively and negatively enriched pathways with a cut-off false discovery rate of $P < 0.25$ were considered significant pathways. The top 20 positively or negatively enriched pathways for each group were then depicted in bar plots based on normalized enrichment scores.

Clonogenic assay

Cells were seeded into six-well plates (3.5×10^5 cells per well) overnight and treated with 10 μM ARS-1620 or 10 μM sonidegib. The medium with drugs was replaced every 3 days. On the indicated day, the media were aspirated, and cells were washed with PBS. A 0.5% crystal violet (Sigma, HT90132), 20% methanol solution was added to the cells. Cells were incubated with

rocking for 30 min, after which the crystal violet was discarded and plates were left to dry overnight.

Chromatin immunoprecipitation assay

Chromatin immunoprecipitation assays were carried out using the EZ-Magna ChIPTM G Kit (Millipore 17-611) according to the manufacturer's instruction. H358 cells were treated with a combination of 10 μM ARS-1620 and 10 μM sonidegib for 48 h. Nuclei were isolated from the cells and sonicated to shear the DNA, which was distributed around 0.2 kb to 1 kb on 1% agarose gel. Chromatin was immunoprecipitated with anti-GLI-1 (Novus, NB 600-600), anti-histone H3 (Cell Signaling, 4620) or an isotype control (Cell Signaling, 2729). The complexes were collected on Protein G Magnetic beads (Invitrogen, 10004D) and subsequently extracted from the beads. Bound DNA was purified and amplified by qPCR with primers that amplify 204-bp (−1262 to −1059), 618-bp (-1078 to -460), 260-bp (-594 to -335), 354-bp (-354 to -1), and 117-bp (−1205 to −1089) regions (Table 1 and Fig. 10) of the KRAS promoter.

Plasmids, small interfering RNAs, transfections, and luciferase assay

The pAuroraA GFP-AURKA-GFP (deposited by Marc Tramier, Institute Genetics & Development of Rennes, Rennes, France) was purchased from Addgene (#157765, addgene.org). The pCMV6-Entry GLI1 was purchased from Origene (RC201110, Rockville, MD, USA). The KRAS promoter reporter pEZX-PG04-KRAS was purchased from GeneCopoeia (HPRM45839-PG04, Rockville, MD, USA). Cells were transfected with plasmid vectors using TurboFect (Thermo Fisher Scientific). Small interfering RNAs (siRNAs) against human AURKA (AURKA-siRNA, ID s195), human GLI-1 (siGLI-1 #1) (GLI-1-siRNA, ID 107671), and control-scrambled siRNA (scRNA, AM4611) were purchased from Thermo

Fisher Scientific. The second siRNA against human GLI-1 (siGLI-1 #2) was synthesized by Integrated DNA Technologies (Coralville, IA) and the sequences were as follows: sense 5'-GCGAAAACAUGUCAAGACAGUGCAT-3', antisense 5'-AUGCACUGUCUUGACAUGUUUUCGCAG-3'. Cells were transfected with siRNA using Lipofectamine RNAiMAX (Invitrogen, 13778150). The expression levels of mRNA were analyzed by qRT-PCR. Luciferase activity was measured using a Secrete-Pair Dual Luminescence Assay kit (GeneCopoeia), according to the manufacturer's instructions, and a SpectraMax L Microplate (Molecular Devices, Sunnyvale, CA, USA). All luciferase assays reported in this study are based on at least three independent experiments, each consisting of three wells per transfection.

Statistical analysis

Differences in the expression of genes were evaluated by Student's t-tests or one-way analysis of variance. A *P* value of less than 0.05 was considered statistically significant.

IV. Results

KRAS^{G12C}-mutant cancer cells initially respond to KRAS^{G12C} inhibitors but rapidly re-express KRAS^{G12C} and reactivate ERK

Acquired resistance against KRAS^{G12C} inhibitors reportedly can be induced by synthesizing new KRAS^{G12C} and reactivating its downstream signaling (18, 19). At first, the time-dependent effects of the KRAS^{G12C} inhibitor ARS-1620 against the expression of KRAS^{G12C}, ERK phosphorylation, accumulation of active KRAS (KRAS-GTP), and the cell cycle of KRAS^{G12C}-mutant lung cancer cells were tested. Consistent with a previous report (18), ARS-1620 initially suppressed ERK phosphorylation and accumulation of KRAS-GTP in both H23 and H358 KRAS^{G12C}-mutant lung cancer cells (Fig. 1A-1D). ARS-1620 also initially arrested the cell cycle at the G1 phase (Fig. 1E). However, both H23 and H358 cells began to express KRAS within 12 h of ARS-1620 treatment (Fig. 1F and 1G), reaccumulate KRAS-GTP, and reactivate ERK over time (Fig. 1A-1D). In addition, by 72 h after ARS-1620 treatment, populations of cells at the S and G2/M phases increased (Fig. 1E). A similar pattern of re-expression of KRAS and reactivation of ERK was observed in both H23 and H358 cells after treatment with another KRAS^{G12C} inhibitor, AMG 510 (Fig. 2). These results suggest that KRAS^{G12C}-mutant lung cancer cells eventually avoid the inhibitory effect of KRAS^{G12C} inhibitors through rapid re-expression of KRAS and reactivation of ERK.

RNA-seq analysis reveals the induction of Hh pathway in KRAS^{G12C}-mutant cancer cells after KRAS^{G12C} inhibitor treatment

To examine the effect of KRAS^{G12C} inhibitors on gene expression profiles in KRAS^{G12C}-mutant cancer cells, RNAs were isolated from H358 cells at 12h and 48h after treatment with the KRAS^{G12C} to conduct RNA-seq analysis. A total of 2,410 differentially expressed genes (DEGs)

(adjusted *P* value < 0.05) with an absolute |log2FC| > 1.5 was detected using DESeq2 (29) in H358 cells treated with ARS-1620 for 12 h and 48 h compared with non-treated cells (Fig. 3) as shown in a heat map (Fig. 4A) and volcano plots (Fig. 3A and 3B). Two-way unsupervised hierarchical clustering of the union of DEGs showed a clear separation of ARS-1620–treated cells from non-treated cells (Fig. 3C). In addition, H358 cells treated with ARS-1620 for 12 h were clearly separated from those treated with ARS-1620 for 48 h (Fig. 3C). Hallmark and Kyoto Encyclopedia of Genes and Genomes (KEGG) gene set enrichment analysis (GSEA) showed that KRAS signaling (Fig. 3D-3E), the cell cycle (Fig. 3F), and the G2/M checkpoint (Fig. 3G) were negatively enriched in H358 cells treated with ARS-1620 for 12 h and 48 h. While the Hh signaling was negatively enriched at 12 h after ARS-1620 treatment by Hallmark GSEA, it was positively enriched at 48 h after ARS-1620 treatment by KEGG GSEA (Fig. 4B-4D).

A comparison of H358 cells treated with ARS-1620 for 48 h against H358 cells treated with ARS-1620 for 12 h identified 1,287 DEGs, with 567 upregulated and 720 downregulated DEGs (adjusted *P* value < 0.05 and an absolute |log2FC| > 1.5), as shown in a volcano plot (Fig. 4E). Hallmark GSEA identified KRAS signaling as the most significantly positively enriched gene set in H358 cells treated with ARS-1620 for 48 h compared with those treated with ARS-1620 for 12 h (Fig. 4F and 4G), indicating that KRAS signaling was upregulated for 48 h after treatment with ARS-1620. In addition, consistent with Fig. 4B–4D, Hh signaling was positively enriched by Hallmark GSEA in H358 cells treated with ARS-1620 for 48 h compared with those treated with ARS-1620 for 12 h (Fig. 4H). Collectively, the results of the RNA-seq analysis suggest that, as indicated in Fig. 1D and 1E, KRAS signaling is initially suppressed but rapidly re-activated in cells treated with $KRAS^{G12C}$ inhibitors. Considering the role of Hh signaling in the expression of genes involved in cell proliferation (30, 31), it is possible that

upregulation of Hh signaling plays a role in upregulating KRAS signaling at 48 h after ARS-1620 treatment. To confirm this hypothesis, RNA-seq analysis was conducted using RNA from H358 cells co-treated with ARS-1620 and the Hh signal inhibitor sonidegib. Hallmark GSEA showed that KRAS signaling was negatively enriched in H358 cells co-treated with ARS-1620 and sonidegib for 48 h compared with those treated with ARS-1620 for 48 h (Fig. 4I and 4J). These results suggest that the Hh signal is at least partly responsible for upregulation of KRAS signals at 48 h after ARS-1620 treatment.

KRAS^{G12C} inhibitors enhance the Hh signal and primary cilia in cancer cells

When an Hh signal is upregulated, GLI transcription factors are activated and induce the transcription of their target genes, such as GLI-1 and PTCH1 (32, 33). Upregulation of Hh signals in GSEA of KRAS^{G12C} inhibitor–treated cells (Fig. 4F-4H) prompted us to test whether KRAS^{G12C} inhibitors increase expression of genes involved in the Hh pathway in cancer cells. Treatment of the KRAS^{G12C} inhibitor ARS-1620 increased the expression of GLI-1, PTCH1, IFT88, and ARL6 in H23 (Fig. 5A–5E) and H358 cells (Fig. 5F–5J). Another KRAS^{G12C} inhibitor, AMG 510, also enhanced the expression of GLI-1, PTCH1, and IFT88 in H23 and H358 cells (Fig. 6). Primary cilia, which are microtubule-based organelles, are required for transduction of Hh signals in vertebrates (21). Hence, the cellular primary cilia membrane markers Arl13b and acetylated α-tubulin (Ac-Tu) were stained to ascertain the potential impact of KRASG12C inhibitors on primary cilia formation. Consistent with Hh signals, immunofluorescent labeling of primary cilia revealed that the proportion of cells exhibiting a cilium and the primary cilia length increased in both H23 (Fig. 5K–5M) and H358 cells (Fig. 5N–5P) after ARS-1620 treatment.

Downregulation of AURKA mediates the induction of Hh signaling and re-expression of KRAS after treatment with a KRAS^{G12C} inhibitor

AURKA plays a key role in primary cilia disassembly (34). AURKA is activated in the G2/M phase, and most AURKA proteins undergo degradation after mitosis (35). The cell cycle of cancer cells treated with KRAS^{G12C} inhibitors has been reported to be arrested at G0/G1 (18). The decrease in AURKA expression in H23 cells (Fig. 7A and 7B) and H358 cells (Fig. 7C and 7D) at 24 h post-treatment, followed by a slight increase at 72 h post-treatment with the KRAS^{G12C} inhibitor ARS-1620, was assessed by analyzing the expression patterns at both mRNA and protein levels in cancer cells. These results suggest that reduced levels of AURKA at 24 h post-treatment may play a role in induction of Hh signals and therefore re-expression of KRAS in cancer cells treated with a KRAS^{G12C} inhibitor. Inhibition of AURKA using siRNA (Fig. 7E-7H) or the inhibitor Tozasertib (Fig. 7I-7K) consistently increased the expression of GLI-1 (Fig. 7F, 7H, 7I, and 7K) and KRAS (Fig. 7G, 7H, 7J, and 7K) in the absence of KRAS^{G12C}-inhibitor treatment.

Whether ectopic expression of AURKA blocks the induction of Hh signal-related genes and the re-expression of KRAS in cancer cells treated with a KRAS^{G12C} inhibitor was investigated. Ectopic expression of AURKA (Fig. 7L) countered the effect of ARS-1620 on induction of GLI-1 (Fig. 7M) and KRAS (Fig. 7N) in H358 cells. Ectopic expression of AURKA also blocked ARS-1620–induced KRAS promoter activity in cancer cells (Fig. 7O). Collectively, these results suggest that downregulation of AURKA in KRAS^{G12C} inhibitor–treated cancer cells induces Hh signaling and re-expression of KRAS.

Inhibition of Hh signals blocks re-expression of KRAS and reactivation of ERK in KRAS^{G12C} inhibitor–treated cancer cells

Considering the role of Hh signaling in the expression of genes involved in cell proliferation (30, 31), it is possible that upregulation of Hh signaling may play a role in re-expression of KRAS in KRAS^{G12C} inhibitor–treated cancer cells. To confirm this hypothesis, RNA-seq was conducted using RNA from H358 cells co-treated with ARS-1620 and Hh signal inhibitor sonidegib. Hallmark GSEA showed that, while KRAS signaling was positively enriched in H358 cells treated with ARS-1620 for 48 h compared with cells treated with ARS-1620 for 12 h (Fig. 4F and 4G), the KRAS signaling was negatively enriched in cells co-treated with ARS-1620 and sonidegib for 48 h compared with cells co-treated for 12 h (Fig. 8A). The RNA-seq results were validated by conducting qRT-PCR amplification and western blot assays. Sonidegib inhibited the induction of genes involved in Hh signaling in ARS-1620-treated H23 (Fig. 8B-8E) and H358 cells (Fig. 8F-8I). This drug also suppressed the formation of primary cilia in H23 (Fig. 8J-8L) and H358 cells (Fig. 8M-8O) after ARS-1620 treatment. Importantly, sonidegib blocked the re-expression of KRAS and reactivation of ERK in both H23 (Fig. 8P and 8Q) and H358 cells (Fig. 8R and 8S), which were detected after ARS-1620 treatment (Fig. 1). In a crystal violet proliferation assay, when cells were treated with ARS-1620 (Fig. 8T) or AMG 510 (Fig. 8U) only, cells had an initial inhibition followed by proliferation (Fig. 8T and 8U). However, combined treatment of a KRAS^{G12C} inhibitor with sonidegib inhibited cell growth until the end of the experiment (Fig. 8T and 8U). Even though sonidegib alone inhibited the formation of primary cilia and the expression of GLI target genes and thus decreased phosphorylation of ERK and cell growth in both H23 and H358 cells (Fig. 9), combination of sonidegib with KRAS^{G12C} inhibitor showed much better inhibitory effect on ERK phosphorylation and cell proliferation than sonidegib alone (Fig. 8, Fig. 9). Taken together,

these result indicate that an Hh signal is required for the re-expression of KRAS, reactivation of ERK, and sonidegib blocks the generation of acquired resistance in cancer cells after treatment with a $KRAS^{G12C}$ inhibitor.

GLI-1 is responsible for reactivation of KRAS induced by $KRAS^{G12C}$ inhibitor in cancer cells

Due to the dependency of the transcriptional programs induced by the Hh signal on the GLI transcription factor (32, 33), whether GLI-1 mediates the re-expression of KRAS in cancer cells treated with a $KRAS^{G12C}$ inhibitor was investigated. GLI-1 binds to the GACCACCCA motif to regulate transcription of target genes (31). A search for transcription-factor binding sites using online software (MatInspector) revealed no putative binding sites for GLI-1 within the *KRAS* promoter region. However, ectopic expression of GLI-1 increased *KRAS* promoter activity in cancer cells without $KRAS^{G12C}$-inhibitor treatment (Fig. 11A), suggesting that GLI-1 plays a role in enhancing KRAS-promotor activity. To determine whether Gli binds to the *KRAS* promoter, the chromatin immunoprecipitation (ChIP) assays in H358 cells transfected with a GLI-1–expressing vector without $KRAS^{G12C}$-inhibitor treatment was performed, *in vitro*. Chromatin was sonicated into fragments and precipitated using isotype control or anti-GLI-1 antibody. The precipitated DNA was subjected to PCR using primers designed to amplify four regions covering the *KRAS* promoter (Fig. 10A and 10B). GLI-1 bound only to the first region of the *KRAS* promoter (−1,262 to −1,059, amplified by KRAS-P1) (Fig. 10A, 10B). Thus, the ChIP assay in H358 cells treated with ARS-1620 was conducted using PCR primers (KRAS-P5) amplifying 117-bp fragment (-1,205 to -1,089) within the first region of *KRAS* promoter. ARS-1620 treatment increased the binding of GLI-1 to the first region of *KRAS* promoter, which was inhibited by sonidegib treatment (Fig. 11B). This indicates that ARS-1620 enhances the binding of GLI-1 to the *KRAS* promoter. To determine whether GLI-1 is required for ARS-

1620–induced KRAS re-expression, H358 cells transfected with siRNA against *GLI-1* were treated with ARS-1620, and KRAS expression was examined. Inhibition of *GLI-1* (Fig. 11C and Fig. 12A) attenuated ARS-1620–induced expression of *PTCH1* (Fig. 11D and Fig. 12B) and *KRAS* mRNA (Fig. 11E and Fig. 12C) and accumulation of KRAS-GTP (Fig. 11F) in H358 cells. Collectively, these data indicate that ARS-1620 enhances GLI-1 binding to the KRAS promoter in cancer cells.

V. Figures

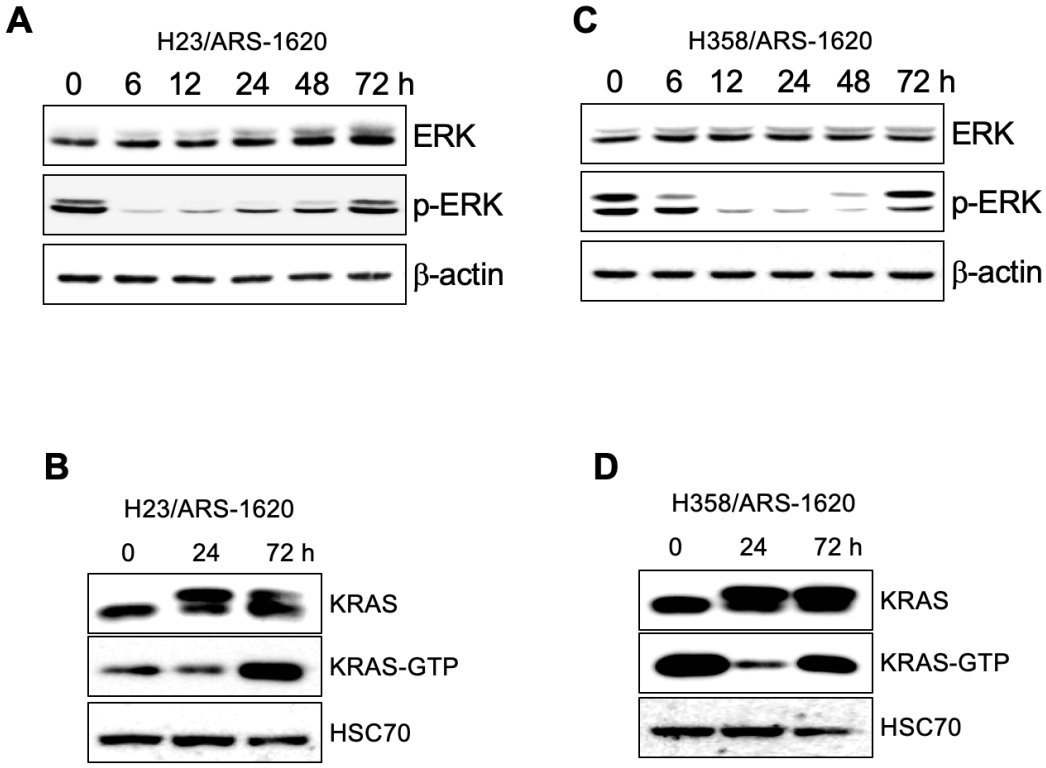
A
H23/ARS-1620
0 6 12 24 48 72 h
ERK
p-ERK
β-actin
C
H358/ARS-1620
0 6 12 24 48 72 h
ERK
p-ERK
β-actin
B
H23/ARS-1620
0 24 72 h
KRAS
KRAS-GTP
HSC70
D
H358/ARS-1620
0 24 72 h
KRAS
KRAS-GTP
HSC70

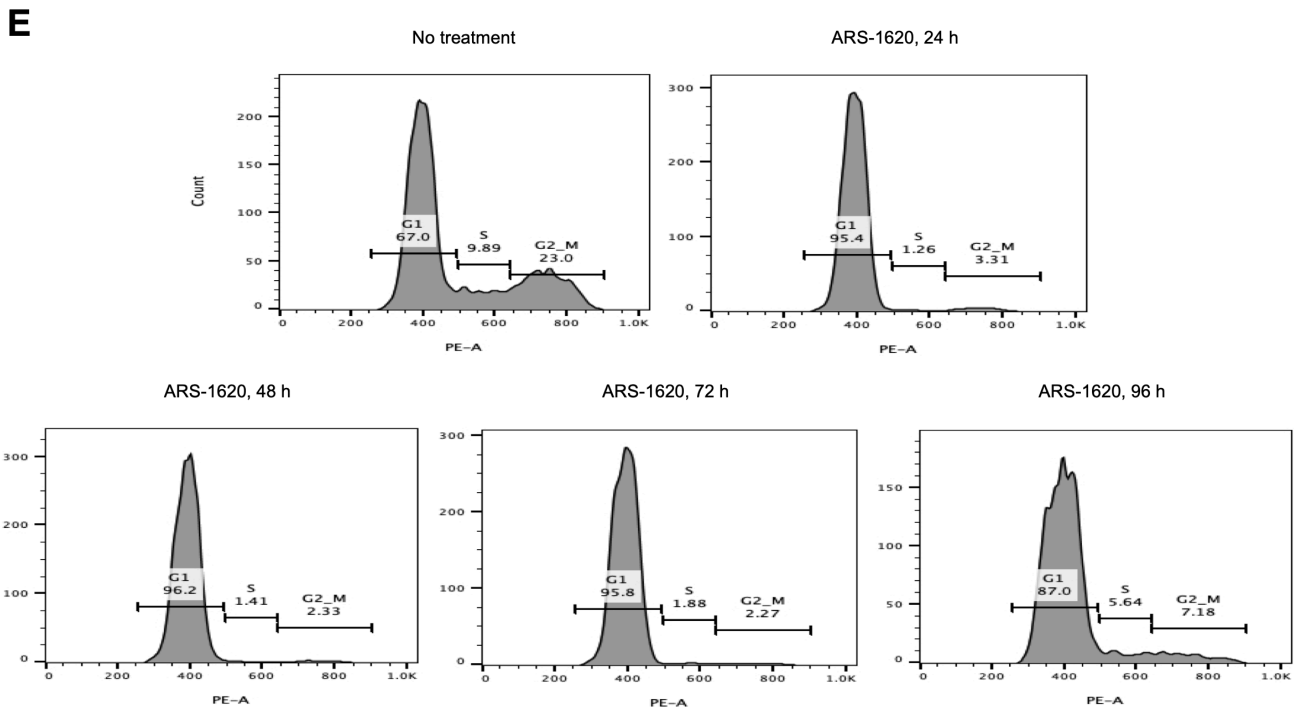
E
No treatment
G1 67.0
S 9.89
G2_M 23.0
ARS-1620, 24 h
G1 95.4
S 1.26
G2_M 3.31
ARS-1620, 48 h
G1 96.2
S 1.41
G2_M 2.33
ARS-1620, 72 h
G1 95.8
S 1.88
G2_M 2.27
ARS-1620, 96 h
G1 87.0
S 5.64
G2_M 7.18
Count
PE-A

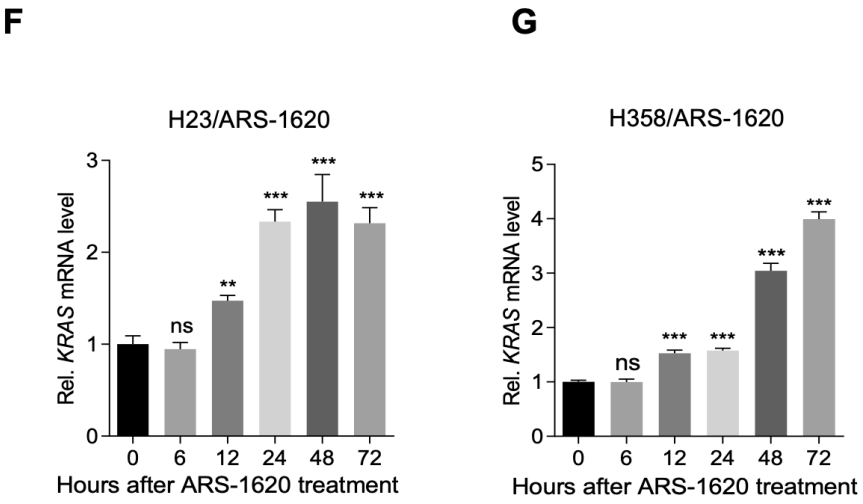

Figure 1. **The KRAS^{G12C} inhibitor ARS-1620 induces re-expression of KRAS and reactivation of ERK signal in lung cancer cells**. (**A**, **B** and **F**) H23 and (**C, D** and **G**) H358 lung cancer cells were treated with 10 μM ARS-1620 for the indicated times. Time-dependent changes in ERK phosphorylation and accumulation of KRAS-GTP in (**A, B**) H23 and (**C, D**) H358 cells were determined by western blot analysis. Time-dependent changes in *KRAS* mRNA levels in (**F**) H23 and (**G**) H358 cells were determined by qRT-PCR. Fold-change in expression level was calculated relative to the values at time 0 for each cell. The graphs are mean ± standard deviation (n = 3 independent experiments) (one-way ANOVA, $^{**}P < 0.01$; $^{***}P < 0.001$). (**E**) Representative plots of flow cytometry using propidium iodide staining for cell cycle analysis of H358 cells. Graphs represent the mean ± standard deviation (n = 3 independent experiments).

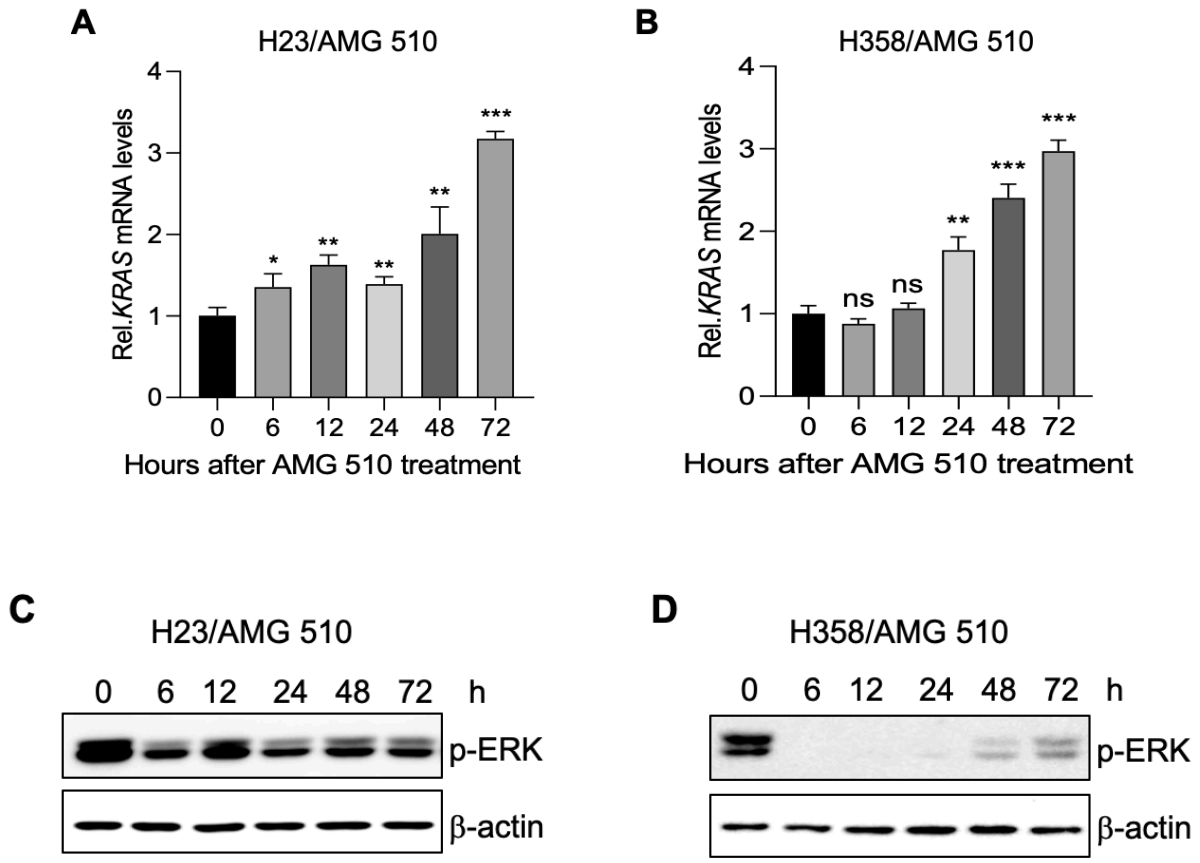

Figure 2. **The KRAS^{G12C} inhibitor AMG 510 induces re-expression of KRAS and reactivation of ERK signal in lung cancer cells**. (**A**, **C**) H23 and (**B**, **D**) H358 lung cancer cells were treated with 0.1 μM AMG 510 for the indicated times. Time-dependent changes in *KRAS* mRNA levels (**A** and **B**) and ERK phosphorylation levels (**C** and **D**) in H23 (**A** and **C**) and H358 (**B** and **D**) cells were determined by qRT-PCR and western blot analysis, respectively. Fold-change in *KRAS* mRNA expression levels was calculated relative to the values at time 0 for each cell. The graphs are mean ± standard deviation of three independent experiments (one-way ANOVA, $^{**}P < 0.01$; $^{***}P < 0.001$).

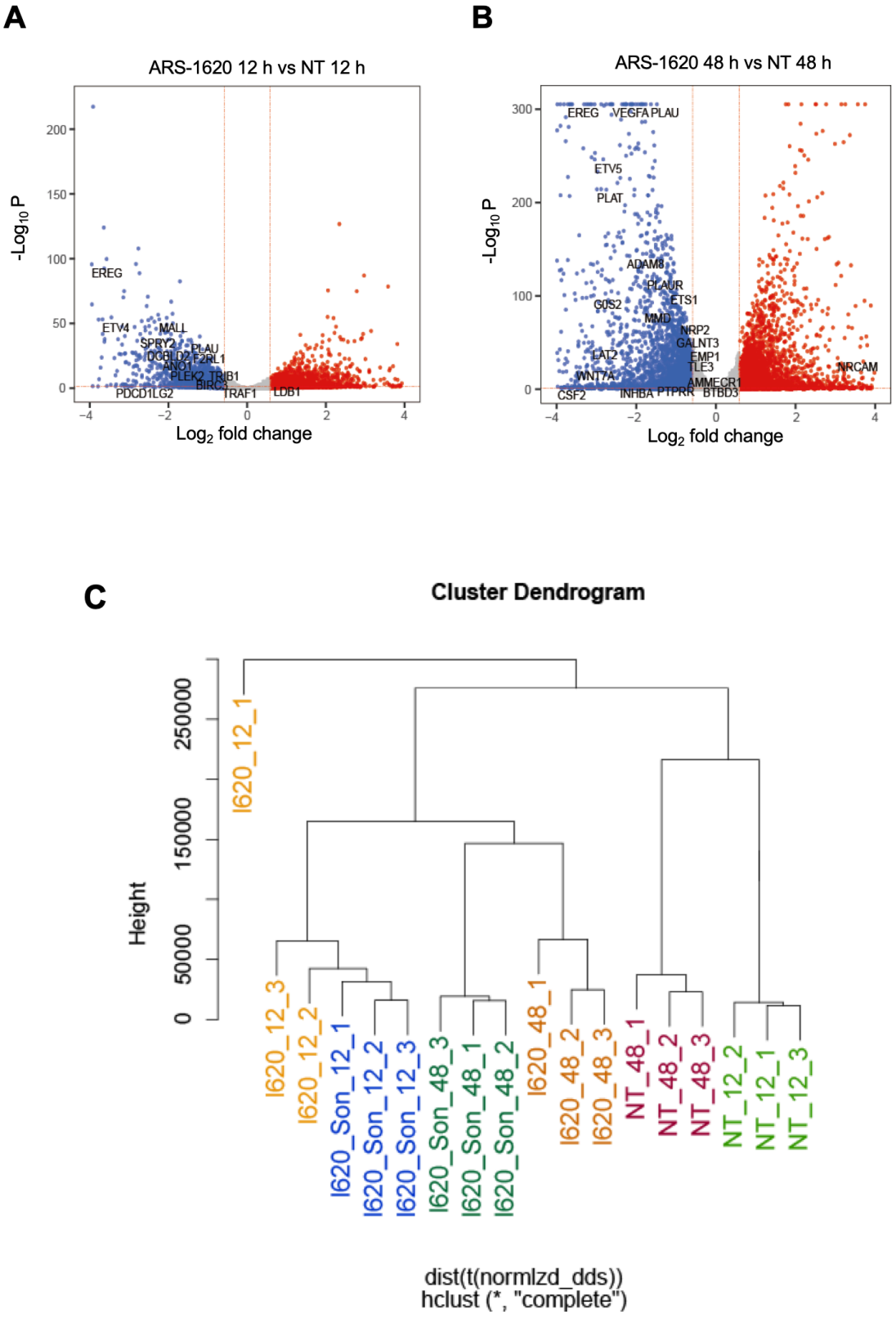
A
ARS-1620 12 h vs NT 12 h
-Log10 P
Log2 fold change
EREG
ETV4
MALL
SPRY2
PLAU
DCBLD2
F2RL1
ANO1
PLEK2
TRIB1
BIRC3
PDCD1LG2
TRAF1
LDB1
B
ARS-1620 48 h vs NT 48 h
-Log10 P
Log2 fold change
EREG
VEGFA
PLAU
ETV5
PLAT
ADAM8
PLAUR
ETS1
GUS2
MMD
NRP2
GALNT3
LAT2
EMP1
TLE3
WNT7A
AMMECR1
NRCAM
CSF2
INHBA
PTPRR
BTBD3
C
Cluster Dendrogram
Height
I620_12_1
I620_12_3
I620_12_2
I620_Son_12_1
I620_Son_12_2
I620_Son_12_3
I620_Son_48_3
I620_Son_48_1
I620_Son_48_2
I620_48_1
I620_48_2
I620_48_3
NT_48_1
NT_48_2
NT_48_3
NT_12_2
NT_12_1
NT_12_3
dist(t(normlzd_dds))
hclust (*, "complete")

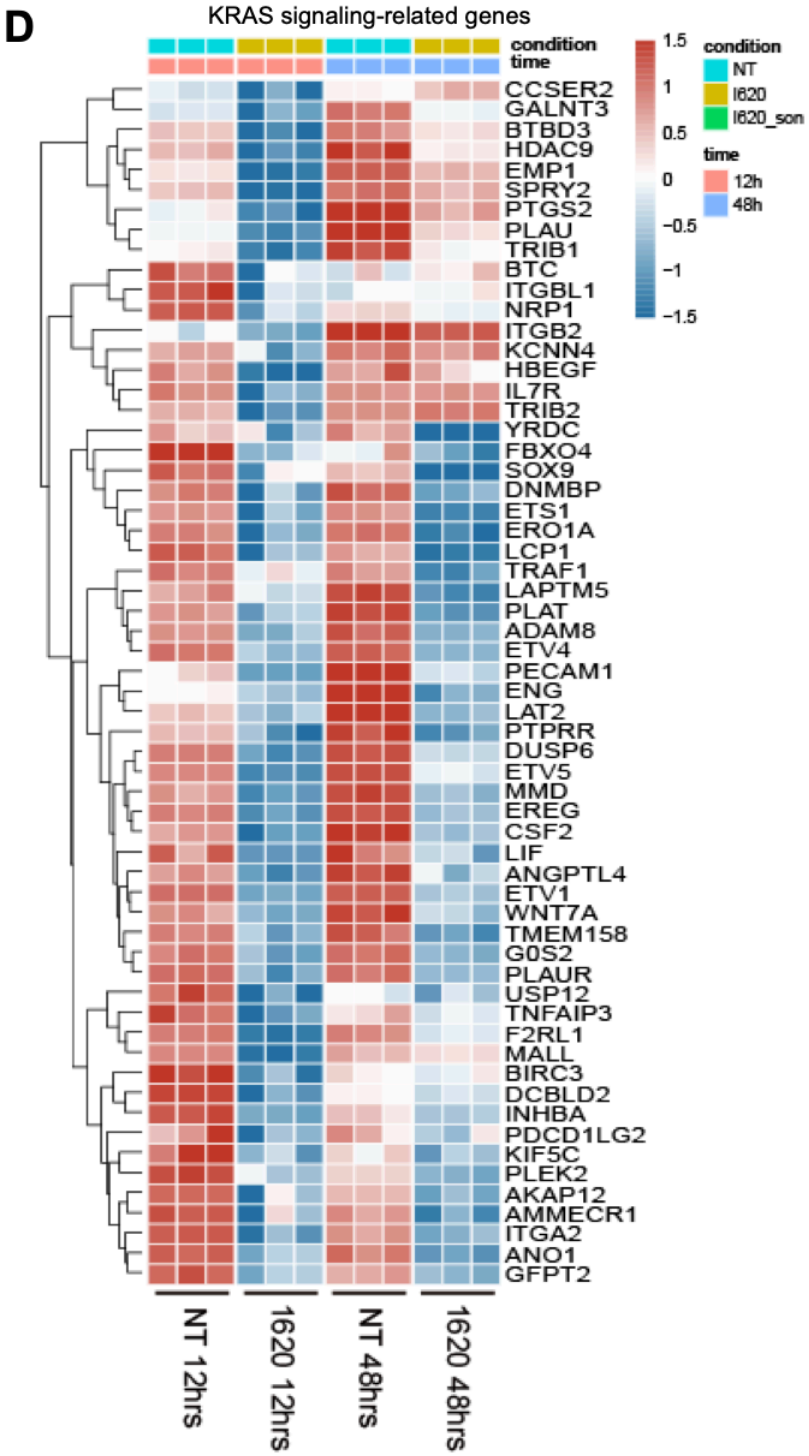
D
KRAS signaling-related genes
condition
time
CCSER2
GALNT3
BTBD3
HDAC9
EMP1
SPRY2
PTGS2
PLAU
TRIB1
BTC
ITGBL1
NRP1
ITGB2
KCNN4
HBEGF
IL7R
TRIB2
YRDC
FBXO4
SOX9
DNMBP
ETS1
ERO1A
LCP1
TRAF1
LAPTM5
PLAT
ADAM8
ETV4
PECAM1
ENG
LAT2
PTPRR
DUSP6
ETV5
MMD
EREG
CSF2
LIF
ANGPTL4
ETV1
WNT7A
TMEM158
G0S2
PLAUR
USP12
TNFAIP3
F2RL1
MALL
BIRC3
DCBLD2
INHBA
PDCD1LG2
KIF5C
PLEK2
AKAP12
AMMECR1
ITGA2
ANO1
GFPT2
NT 12hrs
I620 12hrs
NT 48hrs
I620 48hrs
1.5
1
0.5
0
−0.5
−1
−1.5
condition
NT
I620
I620_son
time
12h
48h

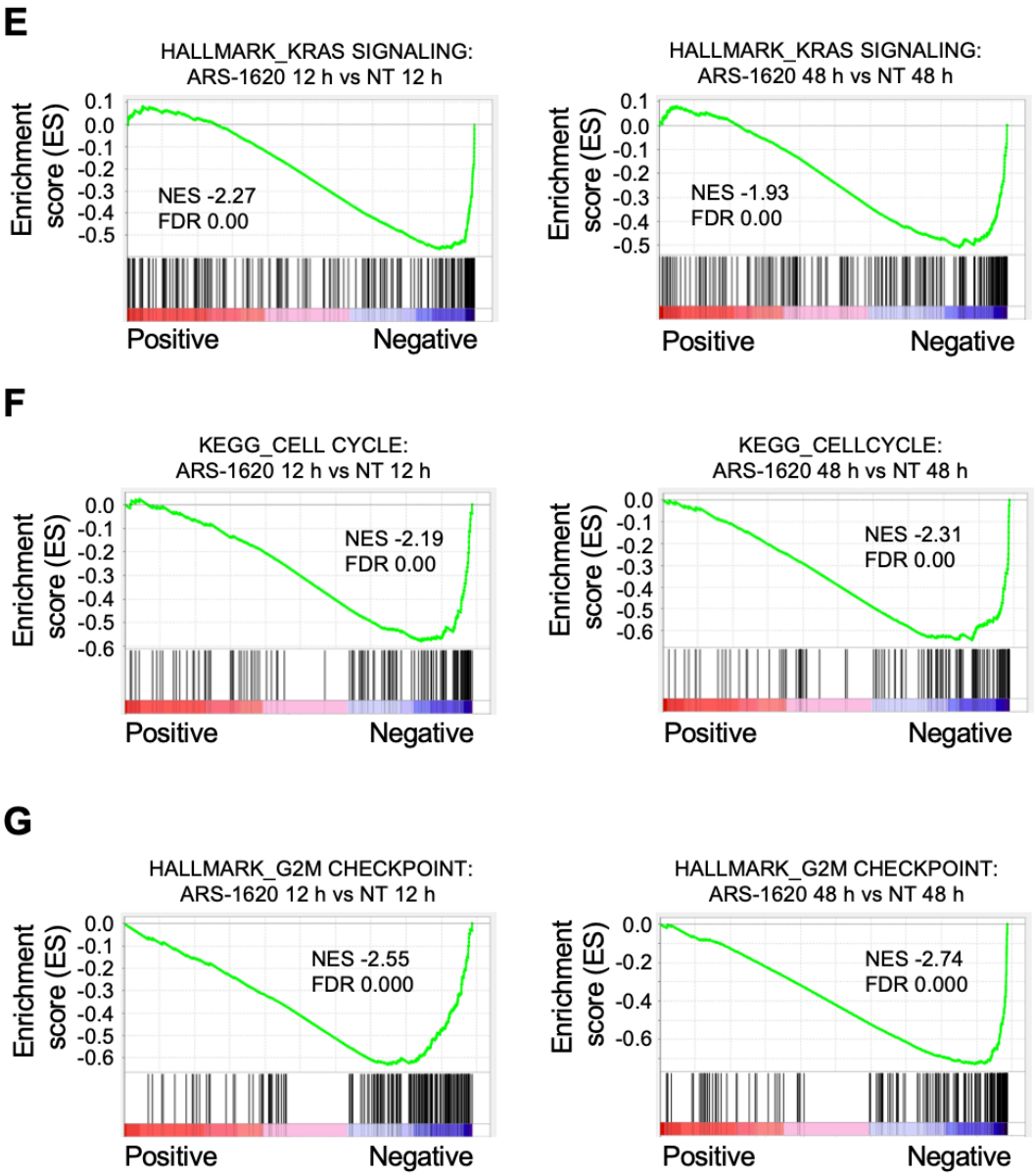

Figure 3. RNA-seq analysis of lung cancer cells after treatment with ARS-1620. H358 cells were treated with a combination of 10 μM ARS-1620 10 μM sonidegib for 12 h or 48 h and their transcriptome profiles were analyzed by RNA-seq. (**A** and **B**) Volcano plots of differentially expressed genes (DEGs) in ARS-1620-treated H358 cells compared with non-treated cells. The y-axis corresponds to the significance level represented with the $-\log_{10}P$ value, and the x-axis displays the $\log_2$ (FC) value. Red dots represent significant (*adj.* $P < 0.05$ and

|log2 FC| ≥ 1.5) DEGs in (**A**) cells treated with ARS-1620 for 12 h and (**B**) cells treated with ARS-1620 for 48 h. A dotted horizontal line indicates an adj. $P = 0.05$, and dotted vertical lines indicate a mean |log2FC| of 1.5. (**C**) Unsupervised hierarchical clustering of RNA-seq data from non-treated cells, cells treated with ARS-1620, and cell treated with ARS-1620 plus sonidegib for 12 h or 48 h (n = 3). (**D**) Heat map of KRAS signaling–related genes. (**E**-**G**) Enrichment plots of KRAS signaling (**E**), cell cycle (**F**), and cell checkpoint (**G**) for negatively enriched ARS-1620-treated cells versus non-treated cells at 12 h and 48 h.

A

947 genes up-regulated at 48 h after ARS-1620 treatment

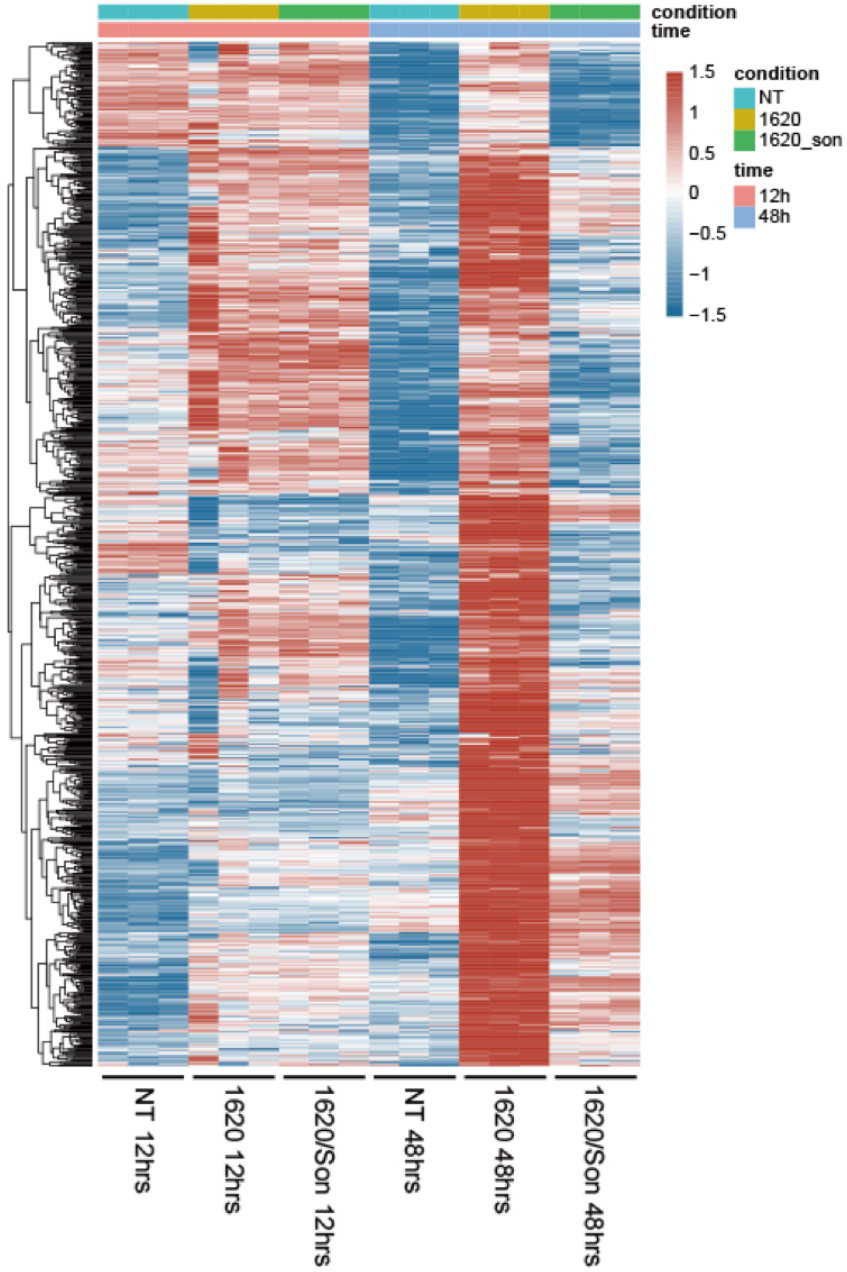

B

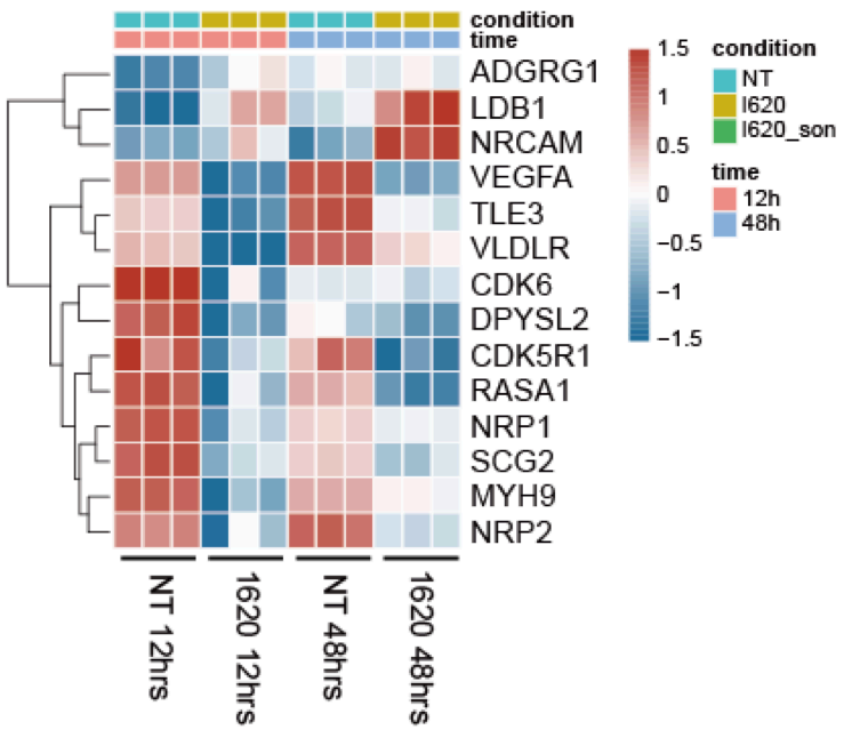
Hedgehog signaling-related genes
condition
time
ADGRG1
LDB1
NRCAM
VEGFA
TLE3
VLDLR
CDK6
DPYSL2
CDK5R1
RASA1
NRP1
SCG2
MYH9
NRP2
NT 12hrs
1620 12hrs
NT 48hrs
1620 48hrs
1.5
1
0.5
0
−0.5
−1
−1.5
condition
NT
I620
I620_son
time
12h
48h

C

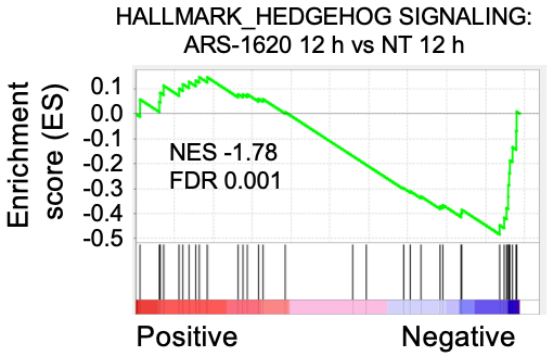
HALLMARK_HEDGEHOG SIGNALING:
ARS-1620 12 h vs NT 12 h
Enrichment score (ES)
0.1
0.0
-0.1
-0.2
-0.3
-0.4
-0.5
NES -1.78
FDR 0.001
Positive
Negative

D

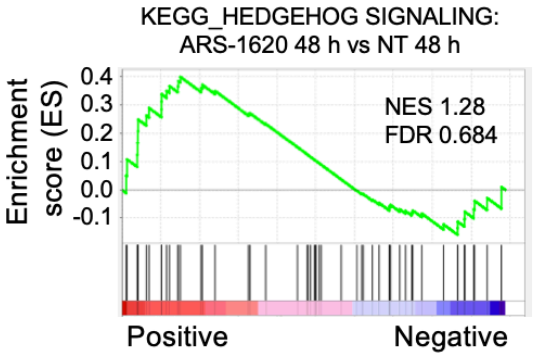
KEGG_HEDGEHOG SIGNALING:
ARS-1620 48 h vs NT 48 h
Enrichment score (ES)
0.4
0.3
0.2
0.1
0.0
-0.1
NES 1.28
FDR 0.684
Positive
Negative

E

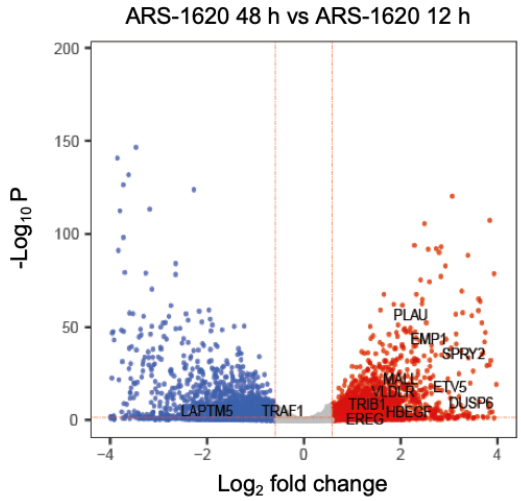
ARS-1620 48 h vs ARS-1620 12 h
-Log10 P
Log2 fold change
PLAU
EMP1
SPRY2
MALL
VLDLR
ETV5
TRIB1
DUSP6
EREG
HBEGF
LAPTM5
TRAF1

F

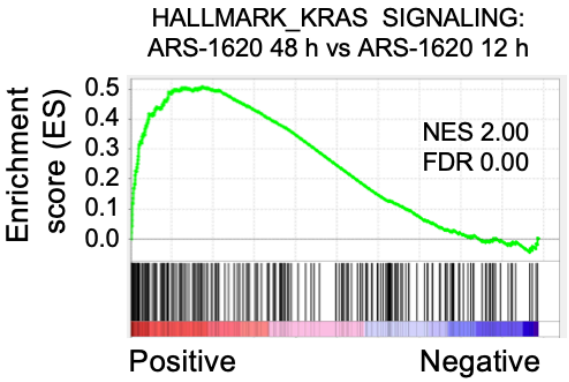
HALLMARK_KRAS SIGNALING:
ARS-1620 48 h vs ARS-1620 12 h
Enrichment score (ES)
NES 2.00
FDR 0.00
Positive
Negative

G

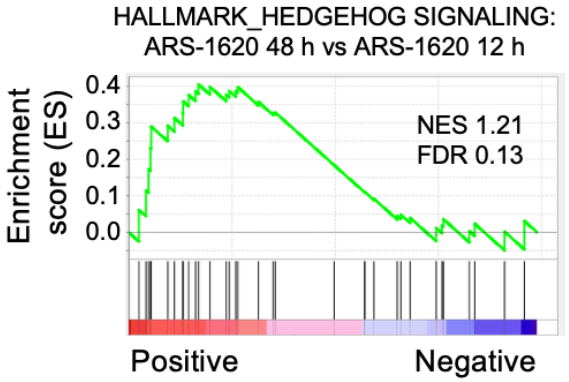
HALLMARK_HEDGEHOG SIGNALING:
ARS-1620 48 h vs ARS-1620 12 h
Enrichment score (ES)
NES 1.21
FDR 0.13
Positive
Negative

H

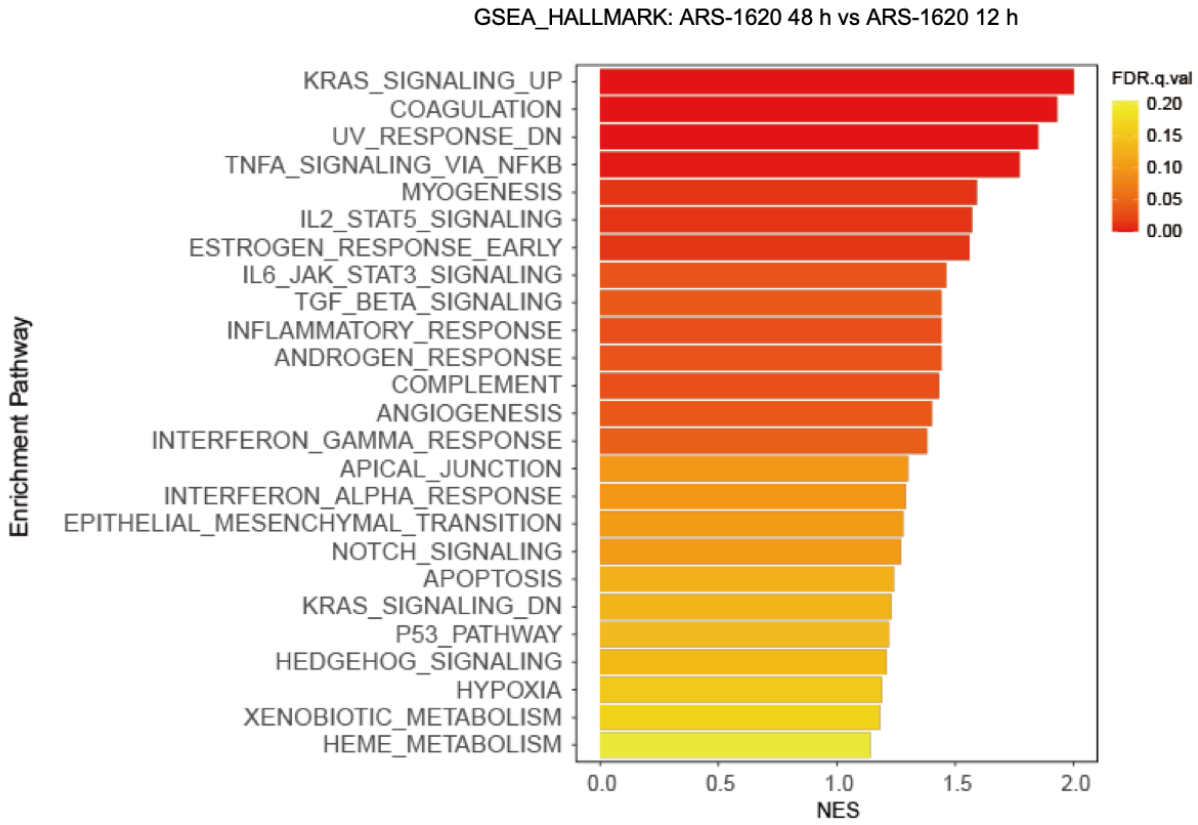
GSEA_HALLMARK: ARS-1620 48 h vs ARS-1620 12 h
KRAS_SIGNALING_UP
COAGULATION
UV_RESPONSE_DN
TNFA_SIGNALING_VIA_NFKB
MYOGENESIS
IL2_STAT5_SIGNALING
ESTROGEN_RESPONSE_EARLY
IL6_JAK_STAT3_SIGNALING
TGF_BETA_SIGNALING
INFLAMMATORY_RESPONSE
ANDROGEN_RESPONSE
COMPLEMENT
ANGIOGENESIS
INTERFERON_GAMMA_RESPONSE
APICAL_JUNCTION
INTERFERON_ALPHA_RESPONSE
EPITHELIAL_MESENCHYMAL_TRANSITION
NOTCH_SIGNALING
APOPTOSIS
KRAS_SIGNALING_DN
P53_PATHWAY
HEDGEHOG_SIGNALING
HYPOXIA
XENOBIOTIC_METABOLISM
HEME_METABOLISM
Enrichment Pathway
FDR.q.val
0.20
0.15
0.10
0.05
0.00
0.0
0.5
1.0
1.5
2.0
NES

I

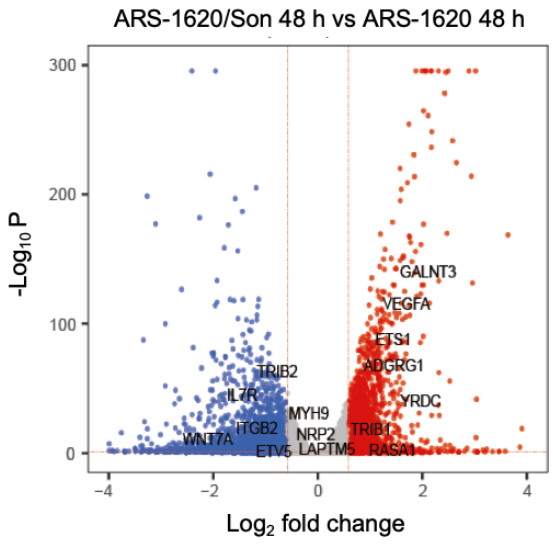
ARS-1620/Son 48 h vs ARS-1620 48 h
300
200
100
0
-Log10 P
GALNT3
VEGFA
ETS1
ADGRG1
YRDC
TRIB1
RASA1
LAPTM5
NRP2
MYH9
TRIB2
IL7R
ITGB2
WNT7A
ETV5
−4
−2
0
2
4
Log2 fold change

J

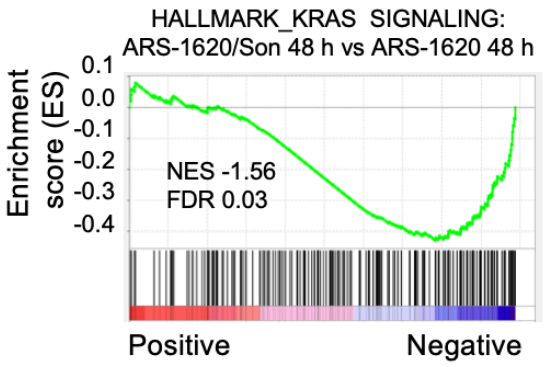
HALLMARK_KRAS_SIGNALING:
ARS-1620/Son 48 h vs ARS-1620 48 h
Enrichment score (ES)
0.1
0.0
-0.1
-0.2
-0.3
-0.4
NES -1.56
FDR 0.03
Positive
Negative

Figure 4. **RNA-seq analysis reveals induced Hedgehog signals in lung cancer cells at 48 h after ARS-1620 treatment.** H358 cells were treated with combination of 10 μM ARS-1620 10 μM sonidegib for 12 h or 48 h and their transcriptome profiles were analyzed by RNA-seq. (**A**) Heat map of 947 genes upregulated at 48 h after treatment with ARS-1620 in H358 cells versus non-treated cells (n = 3 independent experiments). (**B**) Heat map of 14 Hedgehog signaling–related genes. (**C** and **D**) Gene set enrichment plots of Hedgehog signaling (**C**) was negatively enriched in cells at 12 h after ARS-1620 treatment and (**D**) positively enriched in cells at 48 h after ARS-1620 treatment versus non-treated cells. (**E**) Volcano plots of differentially expressed genes (DEGs) in cells treated with ARS-1620 for 48 h compared with cells treated with ARS-1620 for 12 h. The y-axis corresponds to the significance level represented by the $-\log_{10}$P value, and the x-axis displays the $\log_2$ (FC) value. Red dots represent significant (adj. P < 0.05 and |log2FC| ≥ 1.5) DEGs. Dotted horizontal line indicates $P = 0.05$, and the dotted vertical line indicates a mean |log2FC| of 1.5. (**F**–**J**) Gene set enrichment plots of (**F**) KRAS signaling and (**G**) Hedgehog signaling positively were enriched in cells treated with ARS-1620 for 48 h versus cells treated with ARS-1620 for 12 h. (**H**) Bar plot of enriched GSEA pathways in cells treated with ARS-1620 for 48 h versus cells treated with ARS-1620 for 12 h. (**I**) Enrichment plot of KRAS signaling negatively enriched in cells treated with ARS-1620 and sonidegib for 48 h versus cells treated with ARS-1620 for 48 h. (**J**) Bar plot of enriched GSEA pathways in cells treated with ARS-1620 and sonidegib for 48 h versus cells treated with ARS-1620 for 48 h.

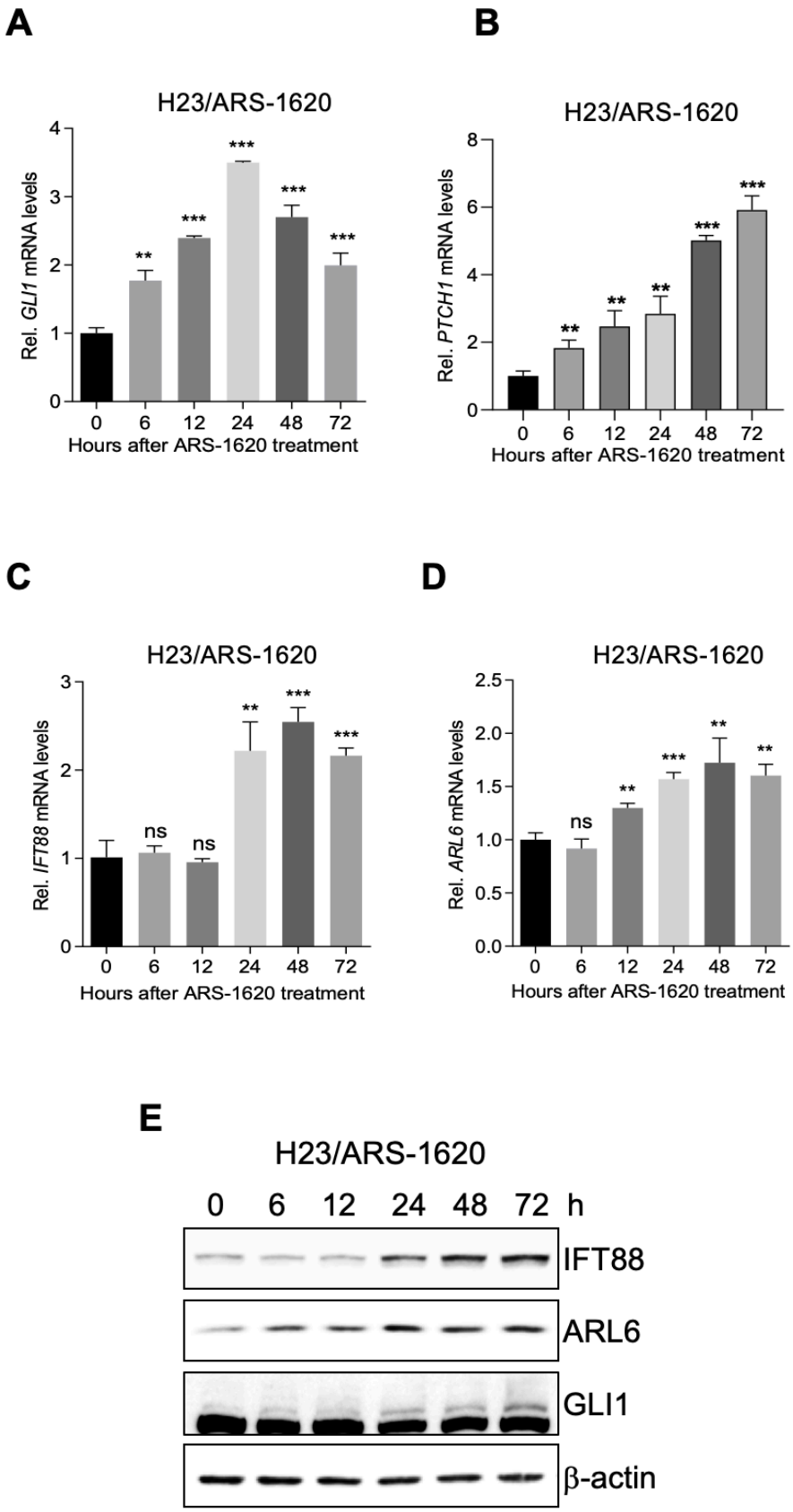
A
H23/ARS-1620
Rel. GLI1 mRNA levels
Hours after ARS-1620 treatment
B
H23/ARS-1620
Rel. PTCH1 mRNA levels
Hours after ARS-1620 treatment
C
H23/ARS-1620
Rel. IFT88 mRNA levels
ns
Hours after ARS-1620 treatment
D
H23/ARS-1620
Rel. ARL6 mRNA levels
ns
Hours after ARS-1620 treatment
E
H23/ARS-1620
0 6 12 24 48 72 h
IFT88
ARL6
GLI1
β-actin

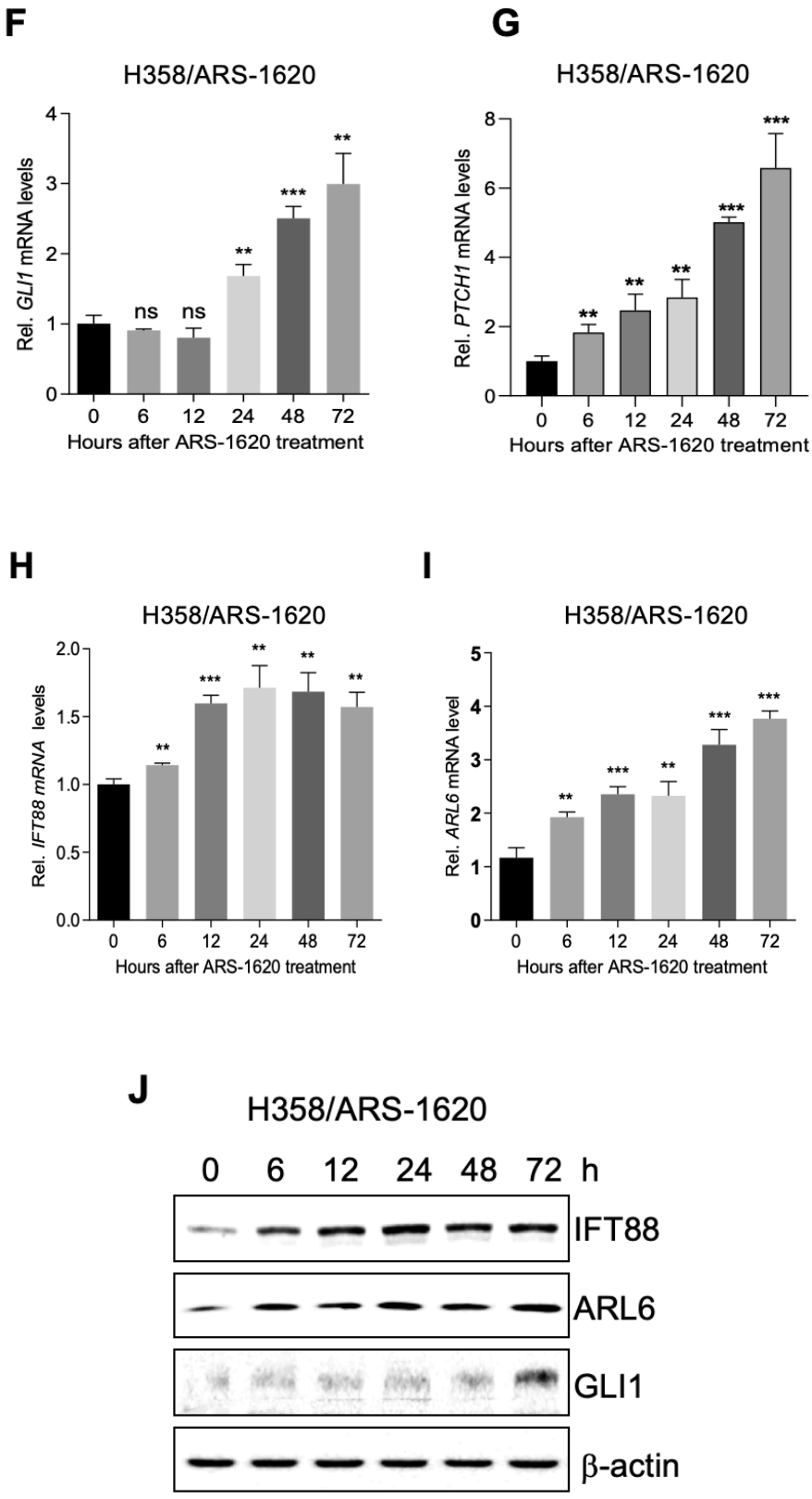
F
H358/ARS-1620
Rel. GLI1 mRNA levels
ns
ns
**
***
**
0 6 12 24 48 72
Hours after ARS-1620 treatment
G
H358/ARS-1620
Rel. PTCH1 mRNA levels
**
**
**
***
***
0 6 12 24 48 72
Hours after ARS-1620 treatment
H
H358/ARS-1620
Rel. IFT88 mRNA levels
**
***
**
**
**
0 6 12 24 48 72
Hours after ARS-1620 treatment
I
H358/ARS-1620
Rel. ARL6 mRNA level
**
***
**
***
***
0 6 12 24 48 72
Hours after ARS-1620 treatment
J
H358/ARS-1620
0 6 12 24 48 72 h
IFT88
ARL6
GLI1
β-actin

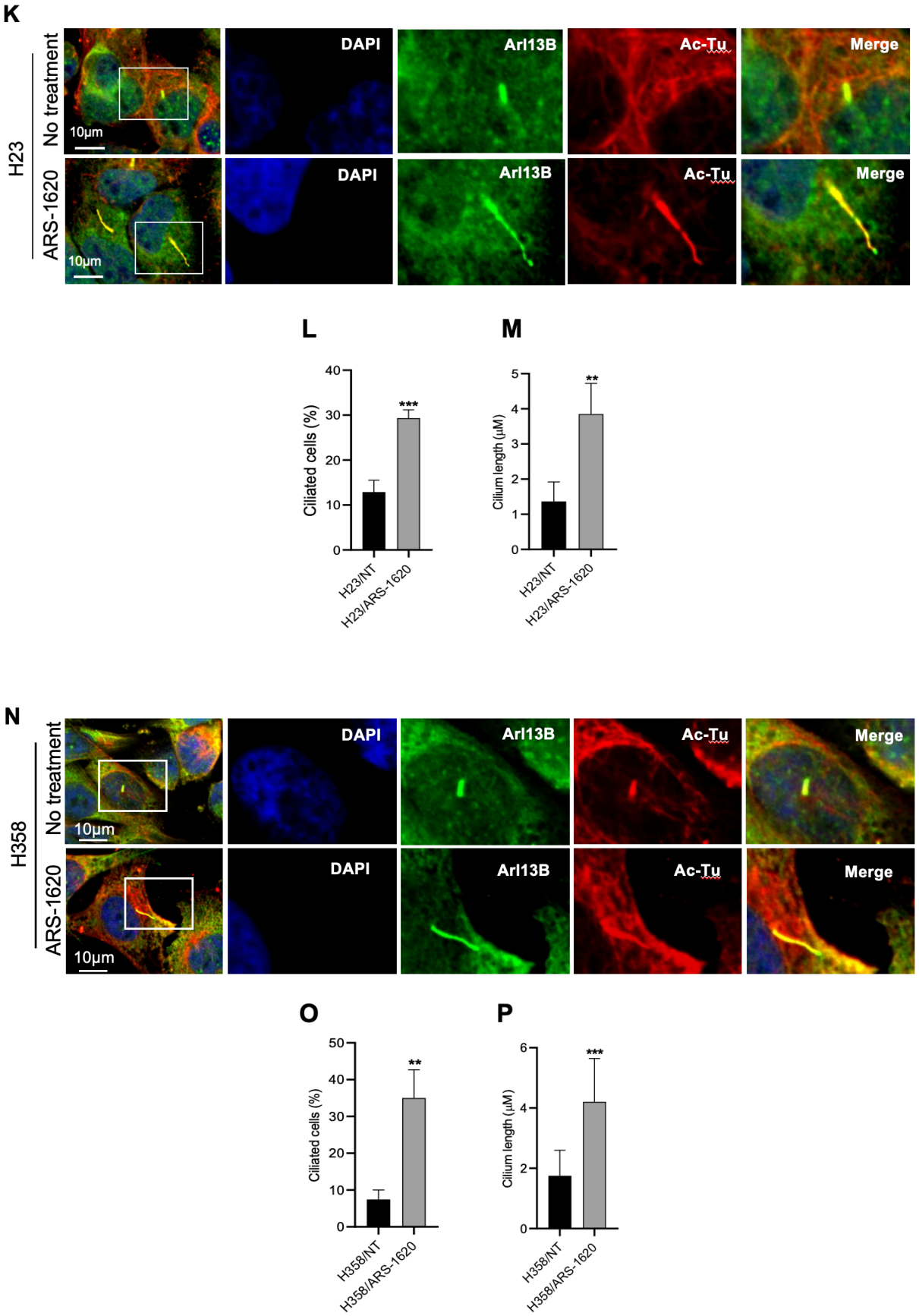
K
H23
No treatment
ARS-1620
10μm
DAPI
Arl13B
Ac-Tu
Merge
L
Ciliated cells (%)
***
H23/NT
H23/ARS-1620
M
Cilium length (μM)
**
N
H358
O
P
H358/NT
H358/ARS-1620

Figure 5. The KRAS^{G12C} inhibitor ARS-1620 induces primary cilia formation and Hedgehog signaling in lung cancer cells. (**A**-**J**) The KRAS^{G12C} inhibitor ARS-1620 enhances Hedgehog signaling in lung cancer cells. (**A**-**E**) H23 and (**F**-**J**) H358 cells were treated with 10 μM ARS-1620 for the indicated times. Time-dependent changes in *GLI-1* (**A** and **F**), *PTCH1* (**B** and **G**), *IFT88* (**C** and **H**), and *ARL6* (**D** and **I**) mRNA levels were determined by qRT-PCR amplification. Fold change in expression levels was calculated relative to the values at time 0 for each cell. The graphs are mean ± standard deviation of three independent experiments (one-way ANOVA, $^{**}P < 0.01$; $^{***}P < 0.001$). Time-dependent changes in ERK phosphorylation in (**E**) H23 and (**J**) H358 cells were determined by western blot analysis. (**K**-**P**) The KRAS^{G12C} inhibitor ARS-1620 induces primary cilia formation in lung cancer cells. (**K**-**M**) H23 and (**N**-**P**) H358 cells were treated with 10 μM ARS-1620 for 72 h and then stained for acetylated tubulin (Ac-Tu, red), Arl13B (green), and DAPI (blue). (**K** and **N**) Representative confocal microscopy images of (**K**) H23 and (**N**) H358 cells. (**L**, **O**, **M**, **P**) Percentages of ciliated (**L**) H23 and (**O**) H358 cells and the average length of cilia of (**M**) H23 and (**P**) H358 cells presented as the mean ± standard deviation (n = 150 pooled from three independent experiments). Student's t-test, $^{*}P < 0.05$; $^{**}P < 0.01$; $^{***}P < 0.001$

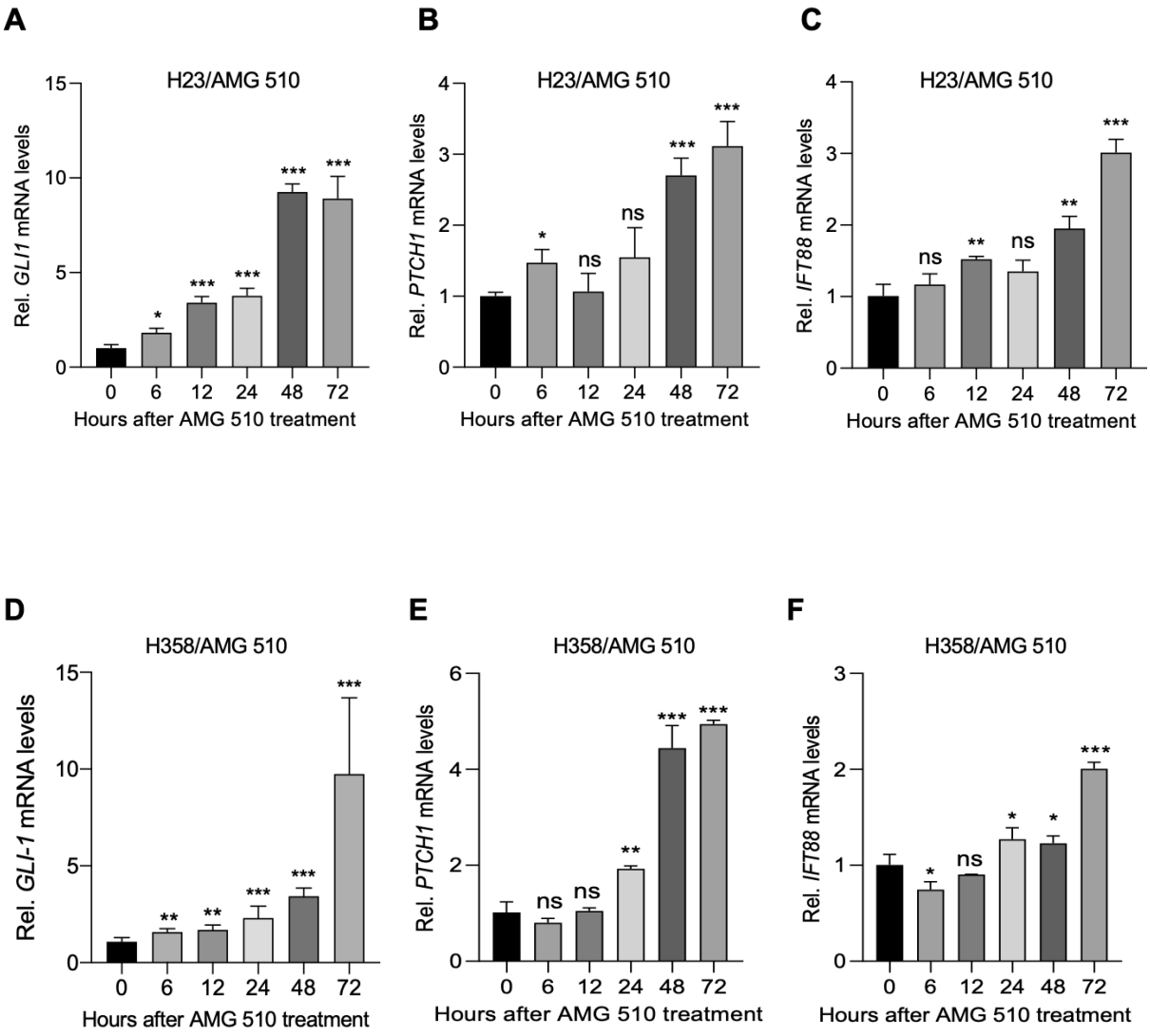

Figure 6. The KRAS^{G12C} inhibitor AMG 510 induces Hedgehog signaling in lung cancer cells. (**A-C**) H23 and (**D-F**) H358 cells were treated with 0.1 μM AMG 510 for the indicated times. Time-dependent changes in *GLI-1* (**A** and **D**), *PTCH1* (**B** and **E**), and *IFT88* (**C** and **F**) mRNA levels were determined by qRT-PCR. Fold change in expression level was calculated relative to the values at time 0 for each cell. The graphs are mean ± standard deviation of three independent experiments (one-way ANOVA, $^{**}P < 0.01$; $^{***}P < 0.001$).

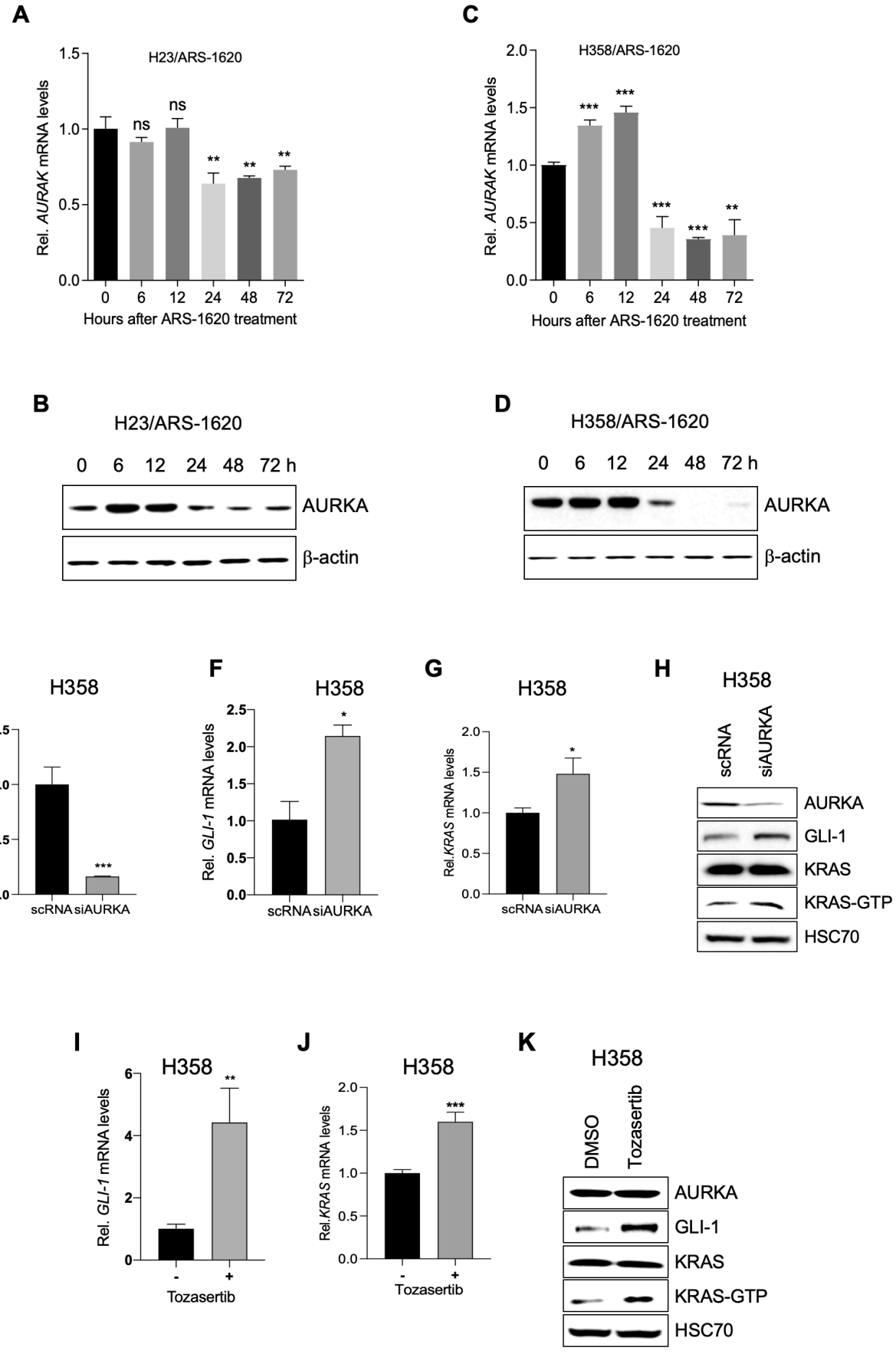
A
H23/ARS-1620
Rel. AURAK mRNA levels
Hours after ARS-1620 treatment
C
H358/ARS-1620
Rel. AURAK mRNA levels
Hours after ARS-1620 treatment
B
H23/ARS-1620
0 6 12 24 48 72 h
AURKA
β-actin
D
H358/ARS-1620
0 6 12 24 48 72 h
AURKA
β-actin
E
H358
Rel. AURKA mRNA levels
scRNA siAURKA
F
H358
Rel. GLI-1 mRNA levels
scRNA siAURKA
G
H358
Rel.KRAS mRNA levels
scRNA siAURKA
H
H358
scRNA
siAURKA
AURKA
GLI-1
KRAS
KRAS-GTP
HSC70
I
H358
Rel. GLI-1 mRNA levels
Tozasertib
J
H358
Rel.KRAS mRNA levels
Tozasertib
K
H358
DMSO
Tozasertib
AURKA
GLI-1
KRAS
KRAS-GTP
HSC70

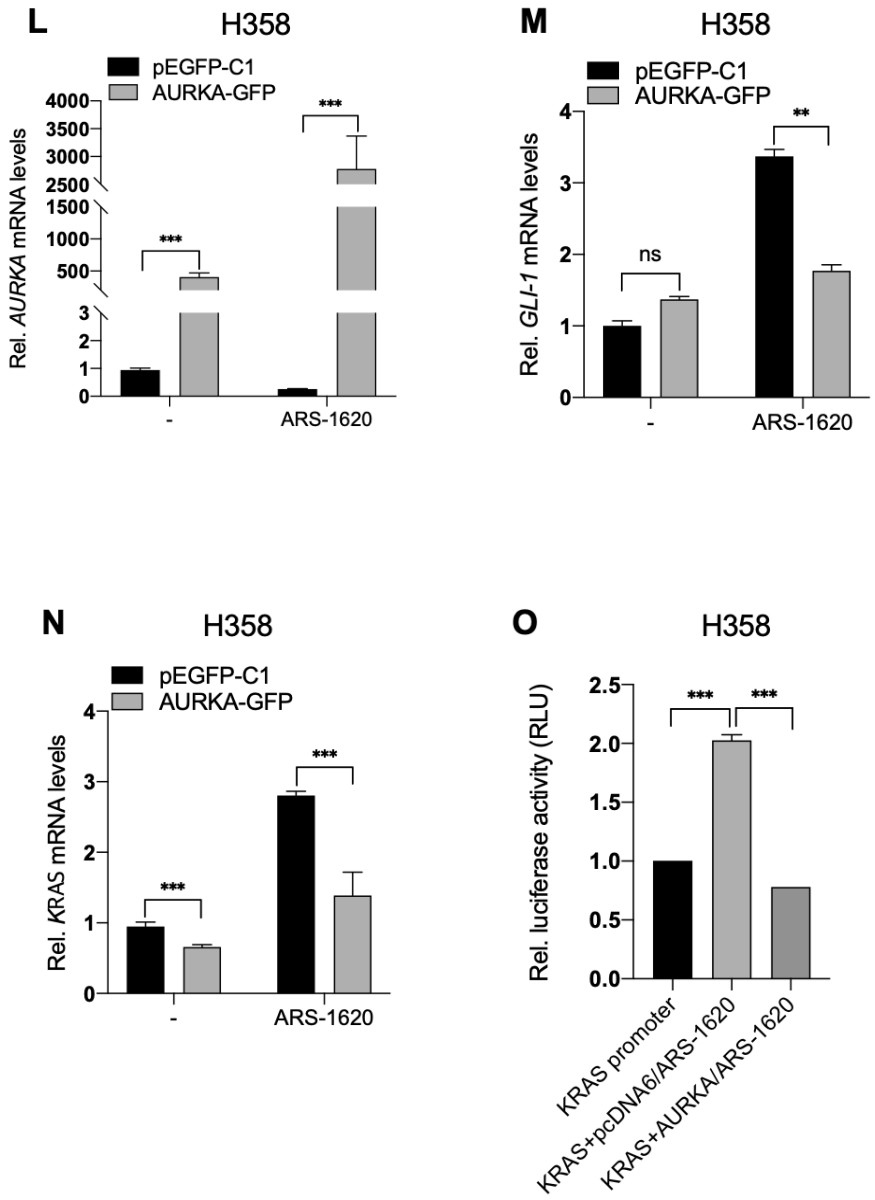

Figure 7. Downregulation of AURKA by ARS-1620 mediates the induction of Hedgehog signaling and re-expression of KRAS. (**A**-**D**) ARS-1620 treatment downregulates the expression of AURKA in lung cancer cells. H23 (**A** and **B**) and H358 (**C** and **D**) cells were treated with 10 μM ARS-1620 for the indicated times. Time-dependent changes in mRNA (**A** and **C**) and protein levels of AURKA (**B** and **D**) were determined by qRT-PCR and western blot analysis, respectively. Fold change in expression levels was calculated relative to the values

at time 0 for each cell. The graphs are mean ± standard deviation of three independent experiments (one-way ANOVA, $**P < 0.01$; $***P < 0.001$). (**E–K**) Inhibition of AURKA using (**E**-**H**) siRNA or (**I**-**K**) an inhibitor (Tozasertib) induced Hedgehog signaling and accumulation of KRAS-GTP. H358 cells were transfected with control scRNA or siRNA against AURKA (siAURKA) or treated with a 10 μM inhibitor. Expression levels of (**E, H,** and **K**) AURKA, (**F, H, I,** and **K**) GLI-1, and (**G, H, J,** and **K**) KRAS were determined by qRT-PCR amplification and Western blot analysis. (**L–N**) Ectopic expression of AURKA attenuates the induction of Hedgehog signals and re-expression of KRAS in ARS-1620-treated cells. H358 cells were transfected with p-Aurora A GFP-AURKA-GFP expression vector or empty vector as a control, followed by treatment with 10 μM ARS-1620 for the indicated times. (**L**) Expression of AURKA was confirmed by qRT-PCR amplification, as were time-dependent changes in (**M**) GLI-1, and (**N**) KRAS mRNAs. Fold-change in expression levels was calculated relative to the values at time 0 for each cell. The graphs are mean ± standard deviation of three independent experiments (one-way ANOVA, $**P < 0.01$; $***P < 0.001$). (**O**) Ectopic expression of AURKA blocks ARS-1620–mediated activation of KRAS promoter. H358 cells were co-transfected with the luciferase reporter vector pEZX-PG04.1/KRAS promoter and p-Aurora A GFP-AURKA-GFP expression vector or empty vector served as a control, followed by treatment with 10 μM ARS-1620 for 48 h. The same volume of dimethylsulfoxide was added to the cells as controls. The fold change in luciferase activity was calculated relative to that of empty vector-transfected dimethylsulfoxide control. The graphs are the mean ± standard deviation of three independent experiments (one-way ANOVA, $***P < 0.001$).

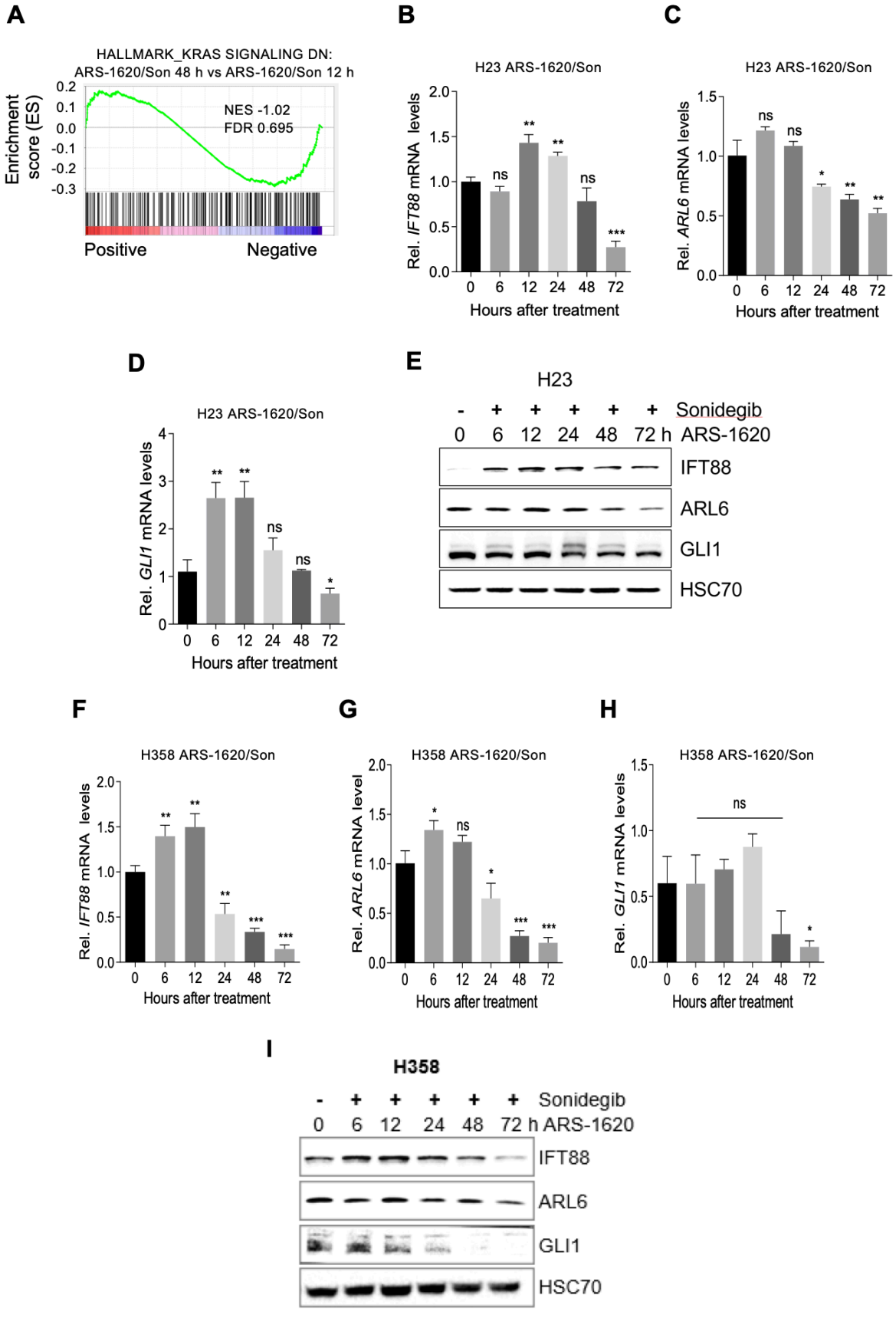
A
HALLMARK_KRAS SIGNALING DN:
ARS-1620/Son 48 h vs ARS-1620/Son 12 h
Enrichment score (ES)
NES -1.02
FDR 0.695
Positive
Negative
B
H23 ARS-1620/Son
Rel. IFT88 mRNA levels
Hours after treatment
C
H23 ARS-1620/Son
Rel. ARL6 mRNA levels
Hours after treatment
D
H23 ARS-1620/Son
Rel. GLI1 mRNA levels
Hours after treatment
E
H23
Sonidegib
ARS-1620
IFT88
ARL6
GLI1
HSC70
F
H358 ARS-1620/Son
Rel. IFT88 mRNA levels
Hours after treatment
G
H358 ARS-1620/Son
Rel. ARL6 mRNA level
Hours after treatment
H
H358 ARS-1620/Son
Rel. GLI1 mRNA levels
Hours after treatment
I
H358
Sonidegib
ARS-1620
IFT88
ARL6
GLI1
HSC70

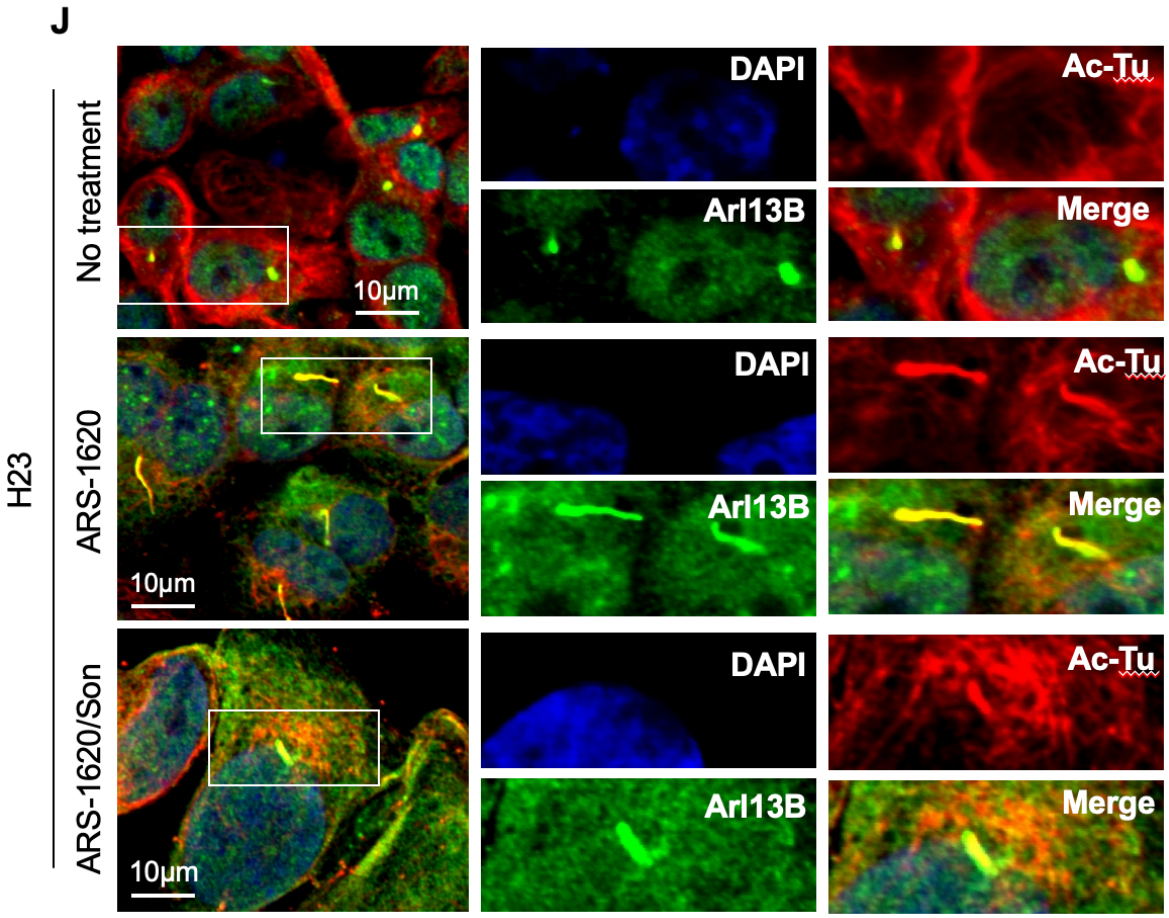
J
H23
No treatment
ARS-1620
ARS-1620/Son
10μm
DAPI
Arl13B
Ac-Tu
Merge

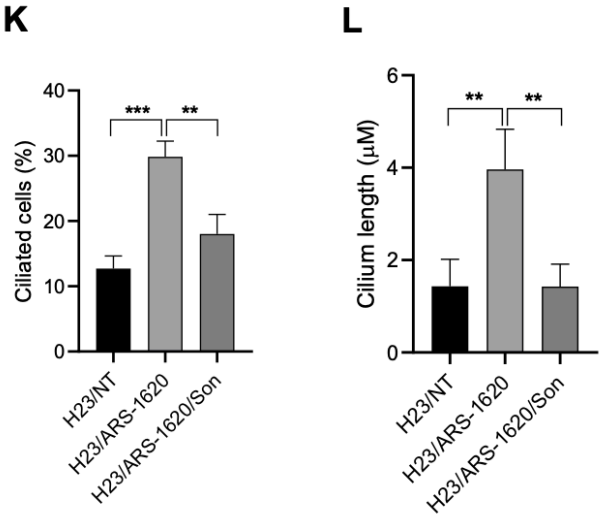
K
L
Ciliated cells (%)
Cilium length (μM)
***
**
H23/NT
H23/ARS-1620
H23/ARS-1620/Son

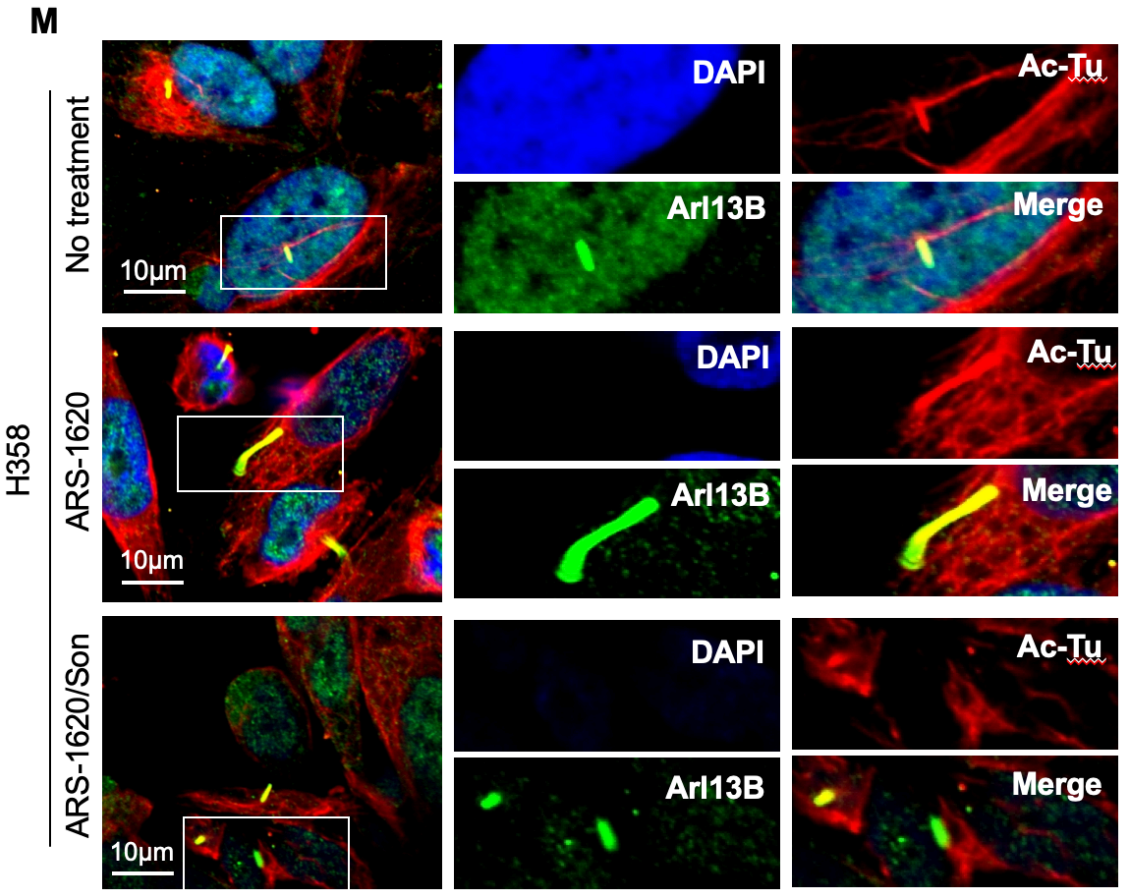
M
H358
No treatment
ARS-1620
ARS-1620/Son
10μm
DAPI
Arl13B
Ac-Tu
Merge

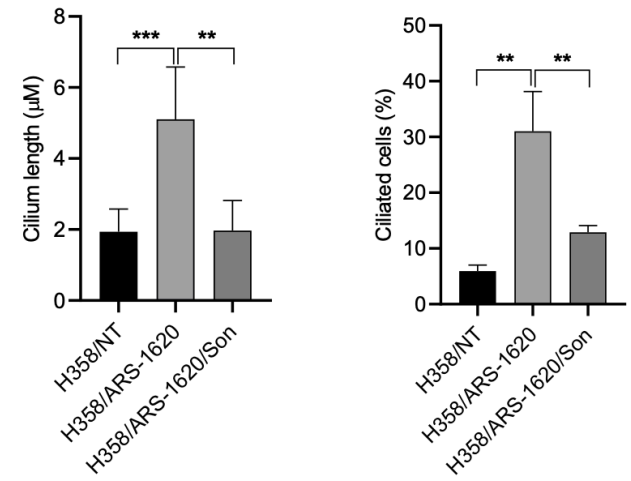
N
Cilium length (μM)
***
**
H358/NT
H358/ARS-1620
H358/ARS-1620/Son

O
Ciliated cells (%)
**
**
H358/NT
H358/ARS-1620
H358/ARS-1620/Son

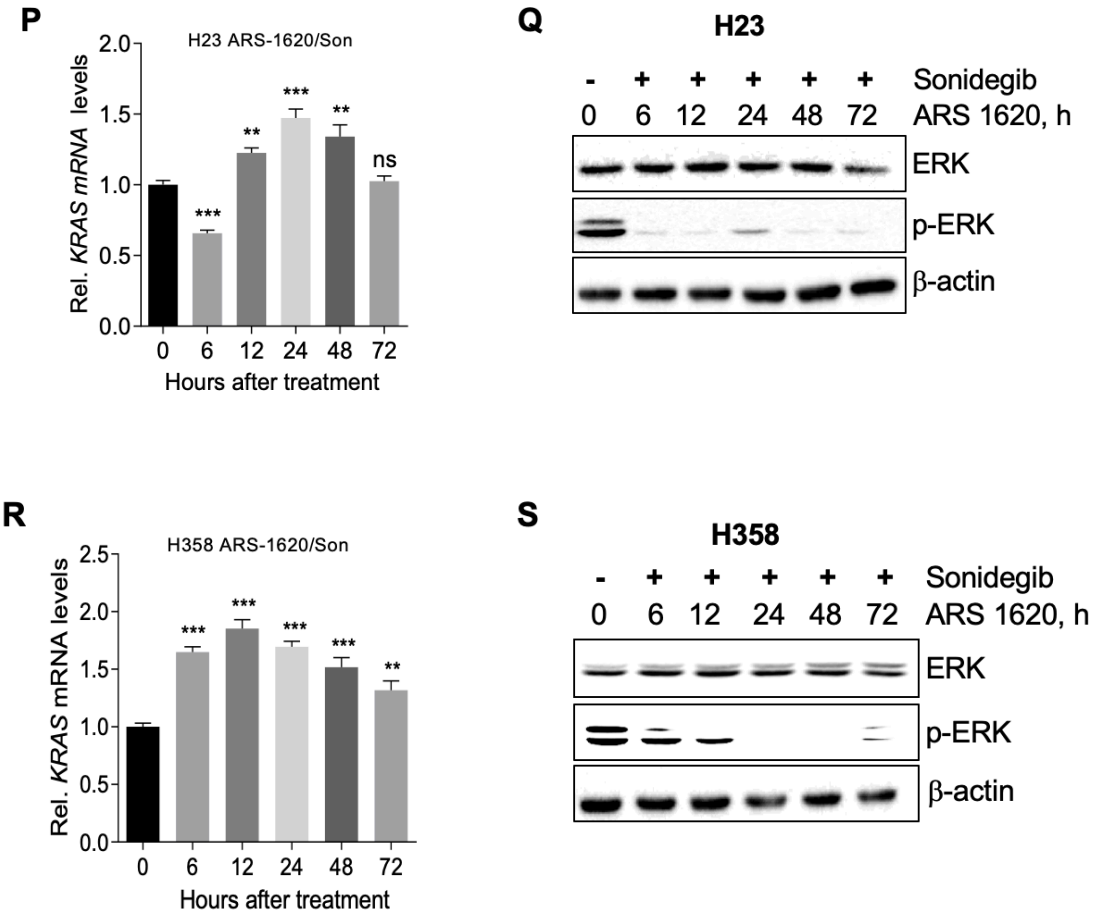
P
H23 ARS-1620/Son
Rel. KRAS mRNA levels
2.0
1.5
1.0
0.5
0.0
***
**
***
**
ns
0 6 12 24 48 72
Hours after treatment
Q
H23
- + + + + + Sonidegib
0 6 12 24 48 72 ARS 1620, h
ERK
p-ERK
β-actin
R
H358 ARS-1620/Son
Rel. KRAS mRNA levels
2.5
2.0
1.5
1.0
0.5
0.0
***
***
***
***
**
0 6 12 24 48 72
Hours after treatment
S
H358
- + + + + + Sonidegib
0 6 12 24 48 72 ARS 1620, h
ERK
p-ERK
β-actin
T
0 1 2 3 5 10 days
H23
No treatment
ARS-1620
Son
ARS-1620/ Son

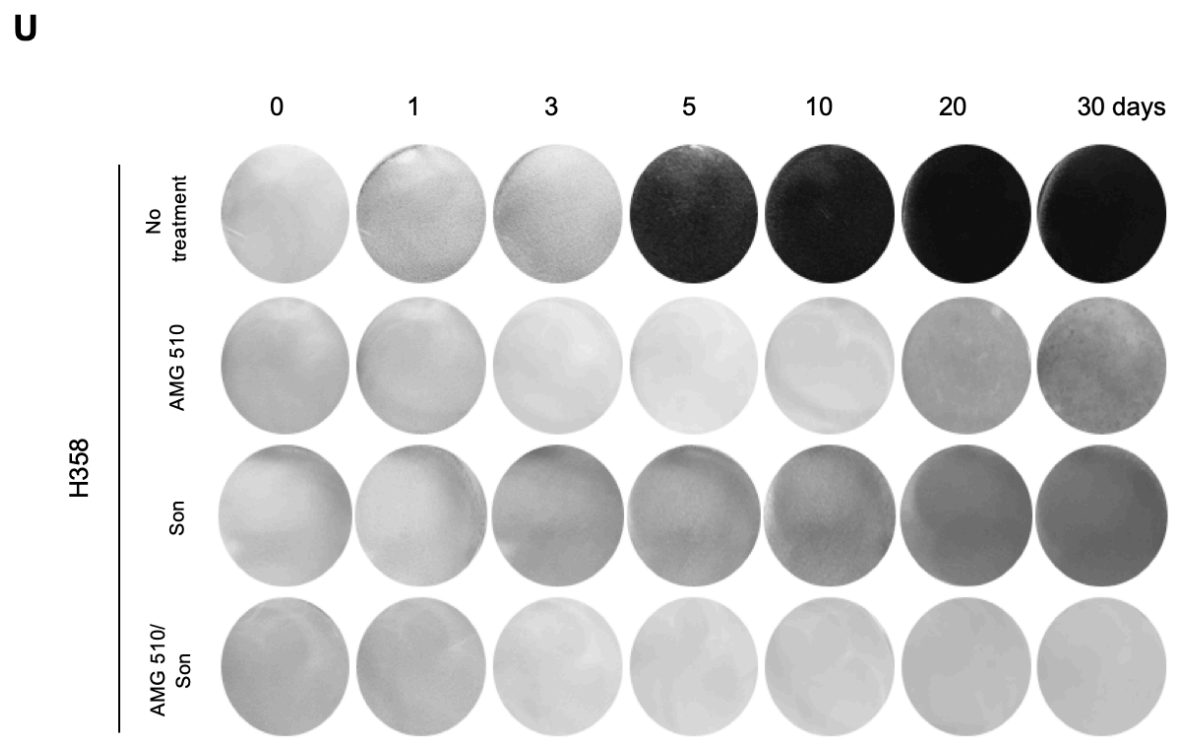

Figure 8. Inhibition of hedgehog signal suppresses re-expression of KRAS and reactivation of ERK in KRAS^{G12C} inhibitor–treated lung cancer cells. H358 cells were co-treated with 10 μM ARS-1620 and 10 μM Smo inhibitor sonidegib for the indicated times. (**A**) Transcriptome profiles were analyzed by RNA-seq as described in **Figure 1** legends. Gene set enrichment plot of KRAS signaling negatively enriched in cells co-treated with ARS-1620 and the Hedgehog signal inhibitor sonidegib for 48 h versus cells treated with ARS-1620 for 48 h. (**B**-**I**) The Smo inhibitor sonidegib suppressed ARS-1620-induced Hedgehog signaling in both (**B**-**E**) H23 and (**F**–**I**) H358 cells. Time-dependent changes in (**B** and **F**) IFT88, (**C** and **G**) ARL6, and (**D** and **H**) GLI-1 mRNA levels were determined by qRT-PCR amplification. Fold change in expression level was calculated relative to the values at time 0 for each cell. The graphs are mean ± standard deviation of three independent experiments (one-way ANOVA, $^{**}P < 0.01$; $^{***}P < 0.001$). Time-dependent changes in IFT88, ARL6 and GLI-1 shown in (**E**)

H23 and (**I**) H358 cells were determined by western blot analysis. (**J**–**O**) The Smo inhibitor sonidegib suppresses ARS-1620-induced primary cilia formation in both (**J**–**L**) H23 and (**M**-**O**) H358 cells. Representative confocal microscopy images of (**J**) H23 and (**M**) H358 cells stained for acetylated tubulin (Ac-Tu, red), Arl13B (green), and DAPI (blue). (**K**, **L**, **N**, **O**) Graphs depict the percentages of ciliated (**K**) H23 and (**N**) H358 cells and average length of cilia of (**L**) H23 and (**O**) H358 cells and are presented as the mean ± standard deviation (n = 150 pooled from three independent experiments). Student's t-tests, $*P < 0.05$; $**P < 0.01$; $***P < 0.001$. (**P**-**S**) The Smo inhibitor sonidegib suppresses ARS-1620–induced re-expression and reactivation of ERK signal in lung cancer cells. Time-dependent changes in *KRAS* mRNA levels in (**P**) H23 and (**R**) H358 cells were determined by qRT-PCR amplification. Fold change in expression level was relative to the values at time 0 for each cell. The graphs are mean ± standard deviation of three independent experiments (one-way ANOVA, $**P < 0.01$; $***P < 0.001$). Time-dependent changes in ERK phosphorylation in (**Q**) H23 and (**S**) H358 cells were determined by western blot analysis (**T** and **U**). The Smo inhibitor sonidegib suppressed the generation of cells resistant to $KRAS^{G12C}$ inhibitors. At the indicated times, (**T**) H23 and (**U**) H358 cells were stained with crystal violet and photographed. Three independent experiments were performed and representative images are shown.

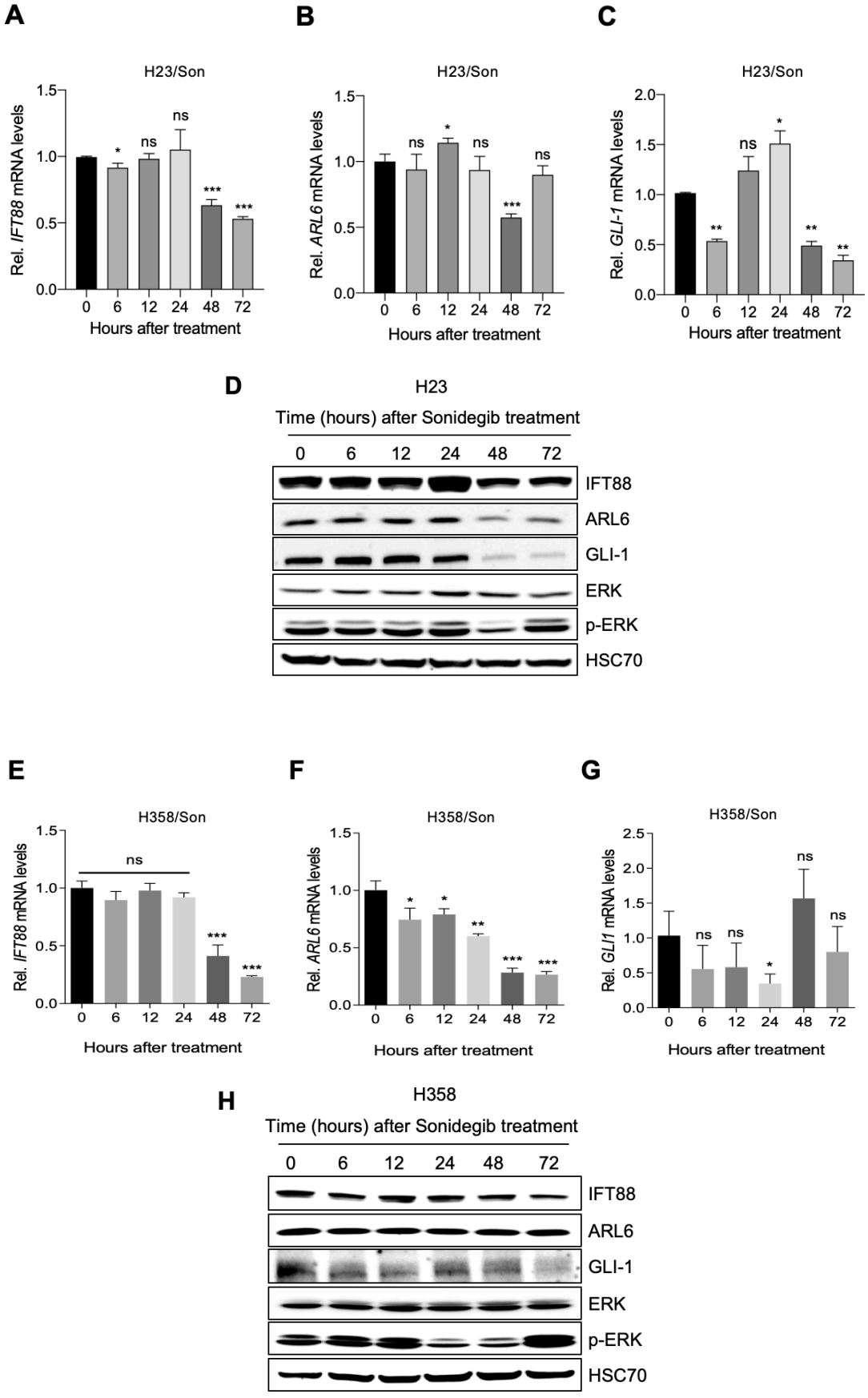
A
H23/Son
Rel. IFT88 mRNA levels
Hours after treatment
B
H23/Son
Rel. ARL6 mRNA levels
Hours after treatment
C
H23/Son
Rel. GLI-1 mRNA levels
Hours after treatment
D
H23
Time (hours) after Sonidegib treatment
IFT88
ARL6
GLI-1
ERK
p-ERK
HSC70
E
H358/Son
Rel. IFT88 mRNA levels
Hours after treatment
F
H358/Son
Rel. ARL6 mRNA levels
Hours after treatment
G
H358/Son
Rel. GLI1 mRNA levels
Hours after treatment
H
H358
Time (hours) after Sonidegib treatment
IFT88
ARL6
GLI-1
ERK
p-ERK
HSC70

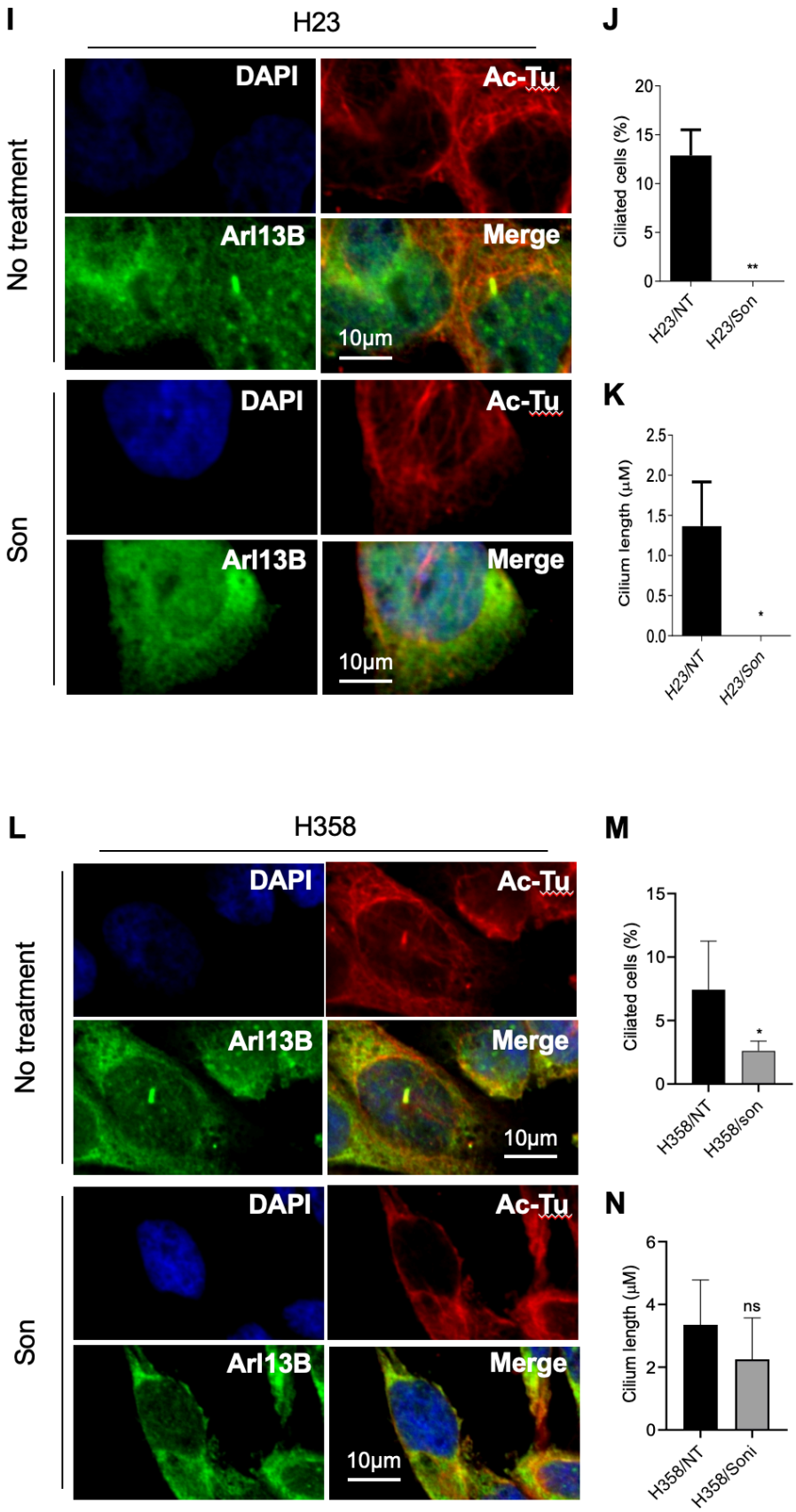
I
H23
No treatment
DAPI
Ac-Tu
Arl13B
Merge
10μm
Son
DAPI
Ac-Tu
Arl13B
Merge
10μm
J
Ciliated cells (%)
20
15
10
5
0
**
H23/NT
H23/Son
K
Cilium length (μM)
2.5
2.0
1.5
1.0
0.5
0.0
*
H23/NT
H23/Son
L
H358
No treatment
DAPI
Ac-Tu
Arl13B
Merge
10μm
Son
DAPI
Ac-Tu
Arl13B
Merge
10μm
M
Ciliated cells (%)
15
10
5
0
*
H358/NT
H358/son
N
Cilium length (μM)
6
4
2
0
ns
H358/NT
H358/Soni

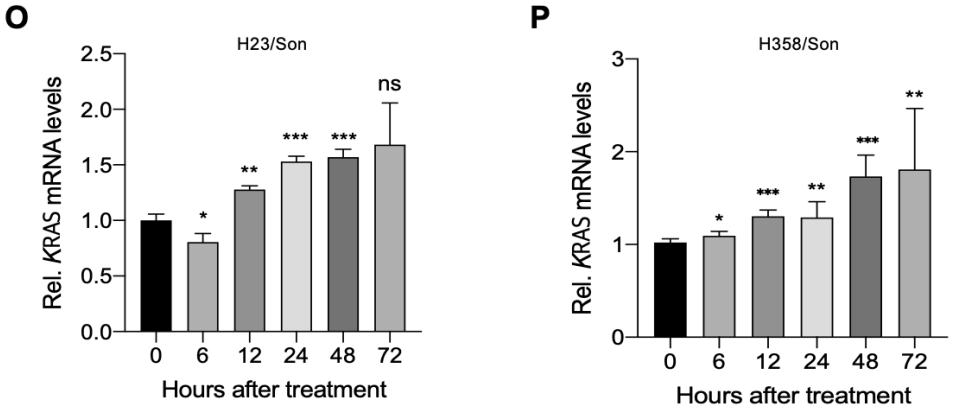

Figure 9. **Effect of Smo inhibitor sonidegib on the hedgehog signal, expression of KRAS, and activation of ERK in lung cancer cells**. (**A-D**) H23 and (**E-H**) H358 cells were treated with 10 μM Smo inhibitor sonidegib for the indicated times. Time-dependent changes in (**A, D, E,** and **H**) IFT88, (**B, D, F,** and **H**) ARL6, (**DC, D, G,** and **H**) GLI-1, and (**D** and **H**) ERK levels were determined by qRT-PCR and Western blot analysis. Fold change in expression level was calculated relative to the values at time 0 for each cell. The graphs are mean ± standard deviation of three independent experiments (one-way ANOVA, $*P < 0.05$; $**P < 0.01$; $***P < 0.001$; ns, not significant). (**I**–**N**) The Smo inhibitor sonidegib suppresses primary cilia formation in both (**I**–**K**) H23 and (**L-N**) H358 cells. Representative confocal microscopy images of (**I**) H23 and (**L**) H358 cells stained for acetylated tubulin (Ac-Tu, red), Arl13B (green), and DAPI (blue). (**J**, **K**, **M**, **N**) Graphs depict the percentages of ciliated (**J**) H23 and (**M**) H358 cells and average length of cilia of (**K**) H23 and (**N**) H358 cells and are presented as the mean ± standard deviation (n = 150 pooled from three independent experiments). Student's t-tests, $*P < 0.05$; $**P < 0.01$; ns, not significant. (**O**, **P**) The effect of Smo inhibitor sonidegib on the expression of *KRAS* mRNA in lung cancer cells. Time-dependent changes in *KRAS* mRNA levels in (**O**) H23 and (**P**) H358 cells were determined by qRT-PCR amplification. Fold change in expression level was relative to the values at time 0 for each cell. The graphs are mean ± standard deviation of

three independent experiments (one-way ANOVA, *$P < 0.05$; **$P < 0.01$; ***$P < 0.001$; ns, not significant).

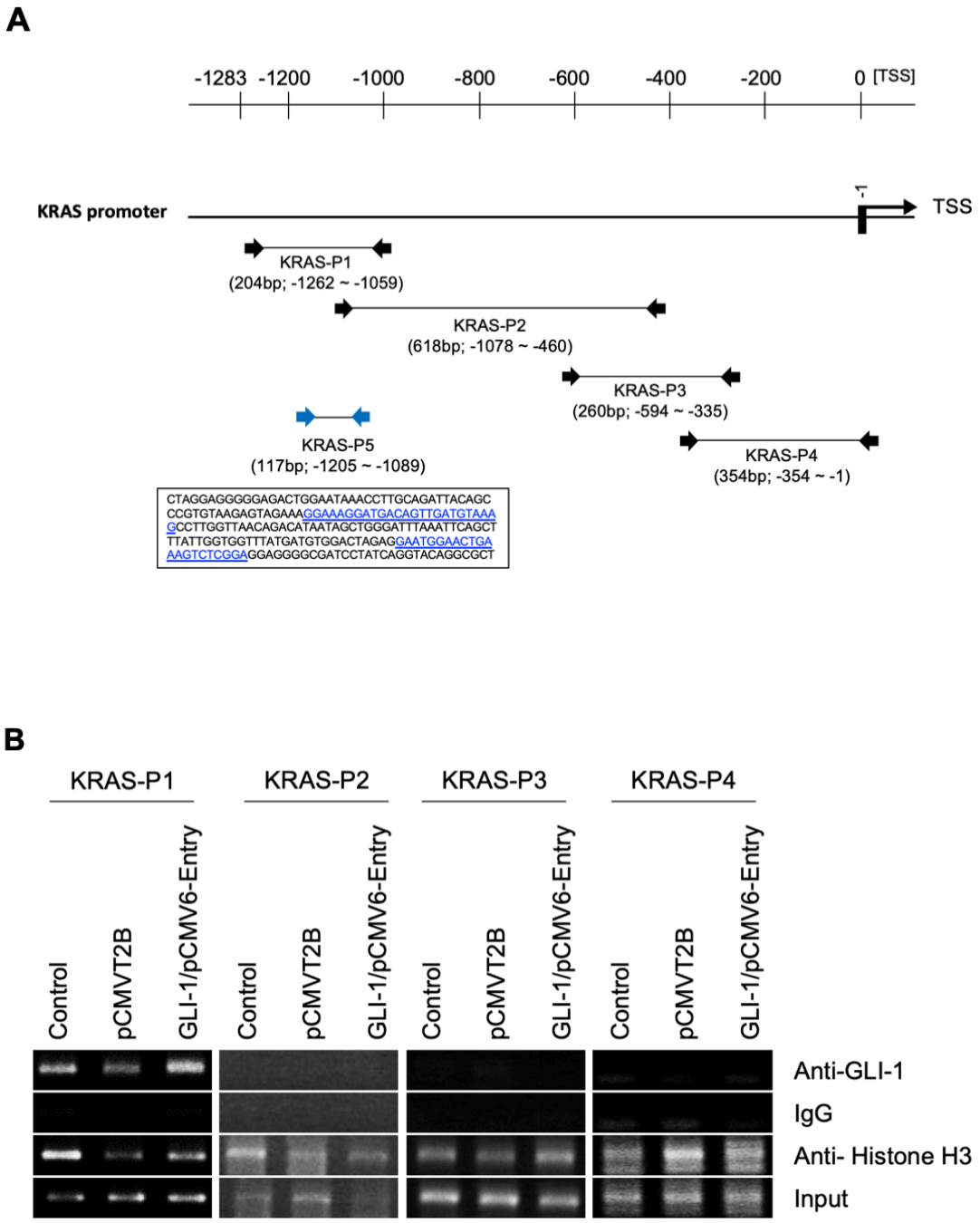

Figure 10. Chromatin immunoprecipitation (ChIP) analysis. (A) The positions of five PCR primer sets on the promoter of the KRAS gene (TSS, transcription start site). The base sequences within the box represent the KRAS promoter region amplified by KRAS-P1. The blue letters within the box represent the positions of KRAS-P5, which was used to generate

ChIP data in Fig. 11B. (B) H358 cells were transfected with a GLI-1 expression vector or empty vector. Control cells were not transfected with any vectors. Formaldehyde-cross-linked chromatin from cells was incubated with anti-GLI-1 antibodies or an immunoglobin G isotype control. Total input DNA at a 1:10 dilution and anti-Histone H3 antibodies were used as positive control for the PCR process. Immunoprecipitated DNA was analyzed by PCR amplification with four sets of primers indicated in (A).

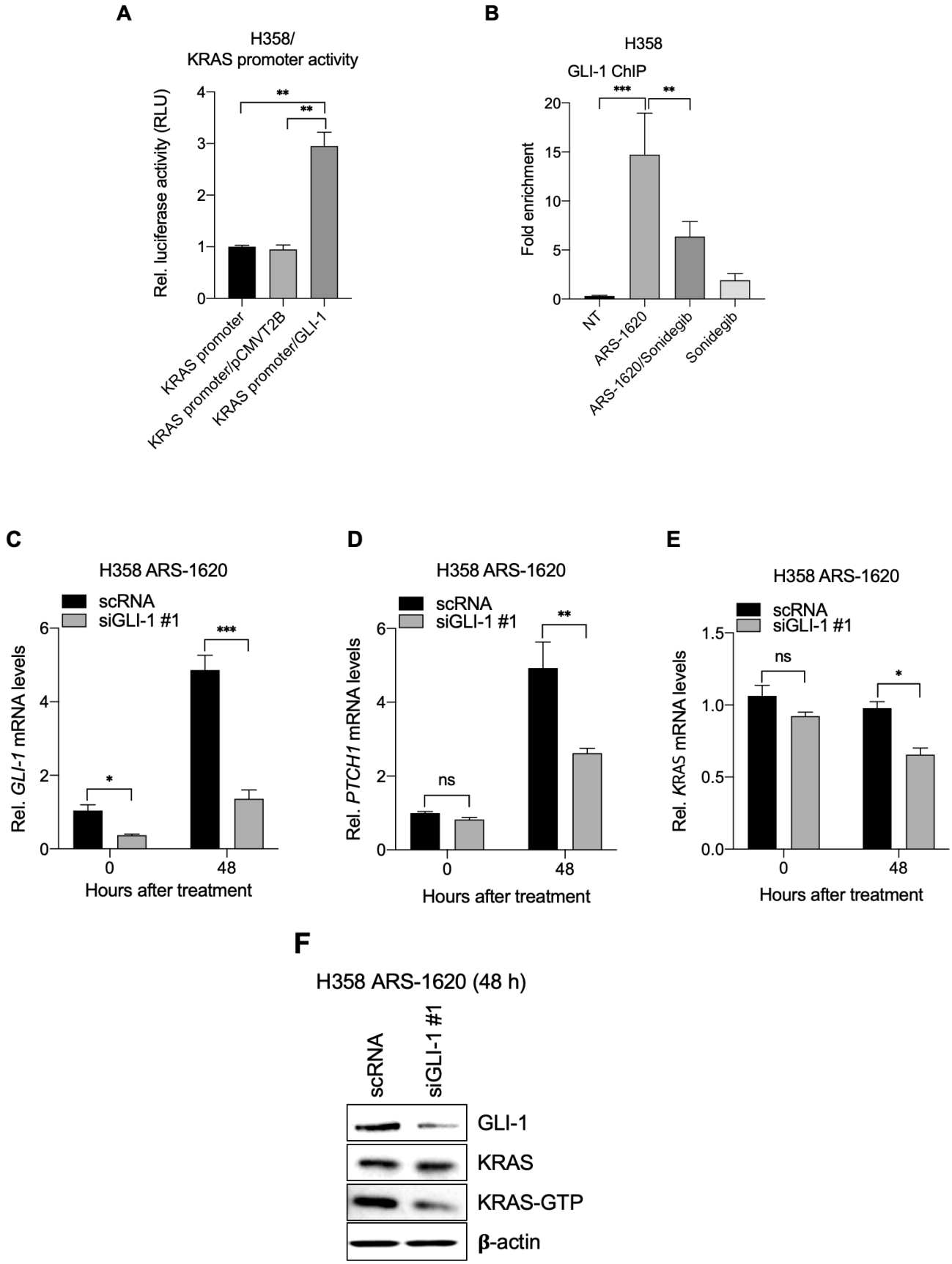
A
H358/
KRAS promoter activity
Rel. luciferase activity (RLU)
KRAS promoter
KRAS promoter/pCMVT2B
KRAS promoter/GLI-1
B
H358
GLI-1 ChIP
Fold enrichment
NT
ARS-1620
ARS-1620/Sonidegib
Sonidegib
C
H358 ARS-1620
scRNA
siGLI-1 #1
Rel. GLI-1 mRNA levels
Hours after treatment
D
H358 ARS-1620
Rel. PTCH1 mRNA levels
E
H358 ARS-1620
Rel. KRAS mRNA levels
F
H358 ARS-1620 (48 h)
scRNA
siGLI-1 #1
GLI-1
KRAS
KRAS-GTP
β-actin

Figure 11. GLI-1 is required to induce KRAS expression in KRAS^{G12C} inhibitor–treated cells. (**A**) Ectopic expression of GLI-1 activates KRAS promoters. H358 cells were co-transfected with the luciferase reporter vector pEZX-PG04.1/KRAS promoter and pCMV6-Entry GLI-1 expression vector, with an empty vector used as a control. The fold change in luciferase activity was calculated relative to that of cells transfected with the pEZX-PG04.1/KRAS reporter vector only. The graphs are mean ± standard deviation of three independent experiments (one-way ANOVA, ***$P < 0.001$). (**B**) GLI-1 binds to the KRAS promoter region. H358 cells were co-treated with 10 μM ARS-1620 and 10 μM sonidegib for 24 h. Chromatin immunoprecipitation–qPCR amplification was conducted to quantitate binding of GLI-1 to KRAS promoter. Fold-enrichment of the KRAS promoter was calculated relative to isotype control. The values represent mean ± standard deviation (n = 3) (one-way ANOVA, ***$P < 0.001$). (**C-F**) Inhibition of GLI-1 attenuates ARS-1620–induced accumulation of KRAS-GTP. H358 cells were transfected with siRNA #1 against GLI-1, followed by 10 μM ARS-1620 treatment for 48 h. Scrambled scRNA was used as a control. Changes in the (**C** and **F**) GLI-1, (**D**) PTCH-1, and (**E** and **F**) KRAS levels were determined by qPCR and Western blot analysis. Fold change in expression levels was calculated relative to the values of scRNA-treated cells at time 0. The graphs are mean ± standard deviation of three independent experiments (one-way ANOVA, *$P < 0.01$; ***$P < 0.001$).

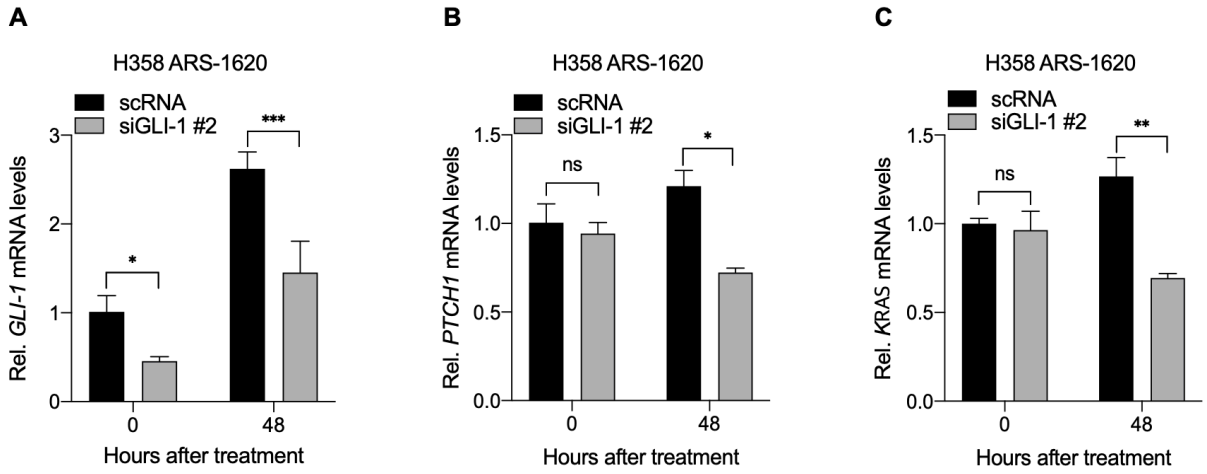

Figure 12. Inhibition of GLI-1 attenuates ARS-1620-induced KRAS expression in lung cancer cells. H358 cells were transfected with siRNA #2 against GLI-1, followed by 10 μM ARS-1620 treatment for 48 h. Scrambled scRNA was used as a control. Changes in the (**A**) *GLI-1*, (**B**) *PTCH-1*, and (**C**) *KRAS* mRNA levels were determined by qPCR. Fold change in expression levels was calculated relative to the values of scRNA-treated

Table 1. PCR primers used in this study

Primers			Sequences (5'-3')
Gene expression analysis	ARL6	F	GGCTTCAAGATCAGATCCAGACT
		R	AAGGTCAGAGTCCATAAATGCAAG
	β-actin	F	ATCGTGCGTGACATTAAGGAGAAG
		R	AGGAAGGAAGGCTGCAAG
	AURKA	F	GCAACCAGTGTACCTCATCCTG
		R	AAGTCTTCCAAAGCCCACTGCC
	GAPDH	F	AATCCCATCACCATCTTCCAG
		R	AAATGAGCCCCAGCCTTC
	GLI1	F	ACAGCCAGTGTCCTCGACTT
		R	ATAGGGGCCTGACTGGAGAT
	IFT88	F	GCCGAAGCACTTAACACTTAT
		R	GTCTAATGCCATTCGGTAGAA
	KRAS	F	TCGACACAGCAGGTCAAGAG
		R	CAAAGAAAGCCCTCCCCAGT
	PTCH1	F	CTCCTTTGCGGTGGACAA
		R	CCTCAGCCTTATTCAGCATTTC
ChIP analysis	KRAS-P1	F	CTAGGAGGGGGAGACTGGAA
		R	AGCGCCTGTACCTGATAGGA
	KRAS-P2	F	TCCTATCAGGTACAGGCGCT
		R	CTCCACAGAGAAGCTGCGAA
	KRAS-P3	F	TAAGTCCCCGAAGTCGCCTC
		R	CTGCCTAGCCGCAAGGCTGT
	KRAS-P4	F	ACAGCCTTGCGGCTAGGCAG
		R	AAATCGAGCTCCGAGCACACCG
	KRAS-P5	F	GGAAAGGATGACAGTTGATGTAAAG
		R	TCCGAGACTTTCAGTTCCATTC

VI. Discussion

$KRAS^{G12C}$ inhibitors have shown promising activity in cancers harboring $KRAS^{G12C}$ (13, 14), but the acquisition of resistance to $KRAS^{G12C}$ inhibitors limits the clinical efficacy of these inhibitors (15). Previously, it has been reported that re-expression of KRAS and reactivation of MAPK pathway can induce acquired resistance against $KRAS^{G12C}$ inhibitors (18, 19). However, the underlying mechanisms of re-expression of KRAS and reactivation of MAPK pathway have not yet been clarified. In this report, the contribution of the Hh signal to the the re-expression of KRAS and reactivation of ERK were observed, and the critical role of the Hh signal on the induction of acquired resistance against $KRAS^{G12C}$ inhibitor in cancer cell was suggested. This study revealed that $KRAS^{G12C}$ inhibitors enhance the formation of primary cilia and Hh signaling, and that inhibition of Hh signaling blocks re-expression of KRAS and reactivation of ERK in lung cancer cells treated with a $KRAS^{G12C}$ inhibitor. In addition, this research provides a molecular basis for how Hh signals induce re-expression of KRAS in cells treated with a $KRAS^{G12C}$ inhibitor, implying that combined treatment of $KRAS^{G12C}$ inhibitors and Hh signal inhibitors may overcome acquired resistance in cancer patients harboring $KRAS^{G12C}$.

The Hh signal activates transcription factor GLI, which in turn induces expression of Hh target genes (26). Among the target genes is *GLI-1* itself (31, 36), which represents a reliable marker for Hh pathway activation (37, 38). These results found that $KRAS^{G12C}$-inhibitor treatment enhanced expression of transcription factor GLI-1 and other GLI-1-target genes, indicating activation of the Hh signal. The transcription factor GLI binds to the consensus sequence GACCACCCA motif to activate Hh target genes (31). However, GLI can bind to non-canonical GLI-binding sites with relatively low affinity, still leading to strong transcriptional activation (39-41). Although the canonical GLI consensus sequence within the promoter region of the KRAS was not detected, GLI bound to the promoter region of KRAS and enhanced

KRAS promoter activity in $KRAS^{G12C}$ inhibitor–treated cells. These results suggest that GLI1 induces the expression of KRAS by binding to a functional non-canonical GLI-binding site (between -1262 and -1059) within the KRAS promoter region. In addition, inhibition of GLI-1 using siRNA suppressed re-expression of KRAS in cells treated with a $KRAS^{G12C}$ inhibitor, indicating that GLI-1 is required for re-expression of KRAS in such cells.

Activation of GLI is triggered by the binding of Hh ligands to their receptor PTCHs (42). The binding of Hh ligands to PTCHs activates Smo (43, 44) and subsequently GLI to upregulate Hh target genes, including factors involved in cell proliferation, survival, self-renewal, and invasiveness (30, 31, 45). RNA-seq analysis revealed that treatment with a $KRAS^{G12C}$ inhibitor did not increase the expression levels of Hh ligands, suggesting that GLI-1 may be activated in the absence of Hh ligands. Several recent studies also have shown that GLI can be activated by oncogenic pathways such as KRAS and TGF-β, independently of the Hh ligand-PTCH1-Smo route in cancer cells (46-48). However, the Smo inhibitor sonidegib suppressed induction of GLI-1 and re-expression of KRAS in $KRAS^{G12C}$ inhibitor–treated cells, suggesting that activation of GLI-1 and re-expression of KRAS occur in a Smo-dependent manner. Further studies are required to clarify the underlying mechanism for activation of GLI-1 in $KRAS^{G12C}$ inhibitor–treated cells.

Transduction of the Hh signal requires the formation of primary cilia, microtubule-based sensory structures (42, 49), which occurs at the G0 or G1 phase of the cell cycle (34, 50). Cell cycle–related kinase AURKA at the basal body of primary cilia stimulates HDAC6-mediated deacetylation and destabilization of microtubules and plays an essential role in the disassembly and resorption of primary cilia (34, 51). AURKA is activated in the late G2 phase and, after mitosis, most AURKA proteins undergo degradation during the G1 phase (35). Considering the role of primary cilia in the transduction of Hh signals (42, 49) and cell cycle arrest of cells

treated with a $KRAS^{G12C}$ inhibitor at G0/G1 phase (18), it is possible that downregulation of AURKA in $KRAS^{G12C}$ inhibitor–treated cells may be responsible for the induction of Hh signaling and re-expression of KRAS. Here these study provide evidence supporting a key role for AURKA in the induction of Hh signaling and re-expression of KRAS in cells treated with a $KRAS^{G12C}$ inhibitor. First, expression levels of AURKA decreased with after treatment with a $KRAS^{G12C}$ inhibitor. Second, inhibition of AURKA using siRNA increased the expression of GLI-1 target genes in the absence of treatment with a $KRAS^{G12C}$ inhibitor. Third, inhibition of AURKA using siRNA also increased the expression of KRAS in the absence of $KRAS^{G12C}$-inhibitor treatment. Fourth, ectopic expression of AURKA blocked the induction of GLI-1 target genes and KRAS re-expression in cells treated with a $KRAS^{G12C}$ inhibitor. However, these results contradicted those of a previous report that suggested AURKA is upregulated in cells with acquired resistance to $KRAS^{G12C}$ inhibitors, and that inhibition of AURKA prevented the reactivation of KRAS (18). *Xue et al.* (18) suggested that AURKA signals can maintain re-expressed $KRAS^{G12C}$ proteins in an active GTP-bound form, facilitating effector activation and cell cycle progression. Like *Xue et al.* (18), the decreased levels of AURKA at 24 h was observed, whereas the rebounded at 72 h after treatment with a $KRAS^{G12C}$ inhibitor. Taken together, it is possible that, at an early time point, $KRAS^{G12C}$ inhibitors arrest the cell cycle at G0/G1, thereby decreasing AURKA expression, which induces primary cilia formation, Hh signaling, and KRAS re-expression. However, at a later time point, re-expressed KRAS promotes cell cycle progress and increases AURKA levels, which maintain the re-expressed $KRAS^{G12C}$ in an active GTP-bound form. An improved understanding of the mechanisms involved in AURKA expression in cells treated with a $KRAS^{G12C}$ inhibitor is required to resolve this discrepancy.

In summary, this study shows that $KRAS^{G12C}$ inhibitors induce formation of primary cilia

and activate Hh signaling, which is responsible for re-expression of KRAS and reacquired resistance against $KRAS^{G12C}$ inhibitors in cancer cells. Several Hh signal inhibitors are used in clinical trials for multiple types of cancers. Most of the efforts to inhibit Hh signaling have been directed at the development of Smo inhibitors. The US Food and Drug Administration and European Medicines Agency have approved two Smo inhibitors, vismodegib and sonidegib, for the treatment of locally advanced or metastatic basal cell carcinoma (52, 53). These study provide evidence that sonidegib suppresses re-expression of KRAS in cancer cells treated with a KRAS inhibitor. These findings extend the understanding of the mechanisms responsible for acquired resistance in cancer cells treated with $KRAS^{G12C}$ inhibitors and indicate that Smo inhibitors are a therapeutic strategy that can overcome acquired resistance against $KRAS^{G12C}$ inhibitors in cancers.

VII. References

1. Milburn MV, Tong L, deVos AM, Brunger A, Yamaizumi Z, Nishimura S, et al. Molecular switch for signal transduction: structural differences between active and inactive forms of protooncogenic ras proteins. Science. 1990;247(4945):939-45.
2. Cully M, Downward J. SnapShot: Ras Signaling. Cell. 2008;133(7):1292- e1.
3. Vetter IR, Wittinghofer A. The guanine nucleotide-binding switch in three dimensions. Science. 2001;294(5545):1299-304.
4. Scheffzek K, Ahmadian MR, Kabsch W, Wiesmuller L, Lautwein A, Schmitz F, et al. The Ras-RasGAP complex: structural basis for GTPase activation and its loss in oncogenic Ras mutants. Science. 1997;277(5324):333-8.
5. Li S, Balmain A, Counter CM. A model for RAS mutation patterns in cancers: finding the sweet spot. Nat Rev Cancer. 2018;18(12):767-77.
6. Kim D, Xue JY, Lito P. Targeting KRAS(G12C): From Inhibitory Mechanism to Modulation of Antitumor Effects in Patients. Cell. 2020;183(4):850-9.
7. Nassar AH, Adib E, Kwiatkowski DJ. Distribution of KRAS (G12C) Somatic Mutations across Race, Sex, and Cancer Type. N Engl J Med. 2021;384(2):185-7.
8. Lito P, Solomon M, Li LS, Hansen R, Rosen N. Allele-specific inhibitors inactivate mutant KRAS G12C by a trapping mechanism. Science. 2016;351(6273):604-8.
9. Downward J. Targeting RAS signalling pathways in cancer therapy. Nat Rev Cancer. 2003;3(1):11-22.
10. Pantsar T. The current understanding of KRAS protein structure and dynamics. Comput Struct Biotechnol J. 2020;18:189-98.
11. Becher I, Savitski MM, Savitski MF, Hopf C, Bantscheff M, Drewes G. Affinity profiling of the cellular kinome for the nucleotide cofactors ATP, ADP, and GTP. ACS Chem Biol.

2013;8(3):599-607.

12. Janes MR, Zhang J, Li LS, Hansen R, Peters U, Guo X, et al. Targeting KRAS Mutant Cancers with a Covalent G12C-Specific Inhibitor. Cell. 2018;172(3):578-89 e17.
13. Canon J, Rex K, Saiki AY, Mohr C, Cooke K, Bagal D, et al. The clinical KRAS(G12C) inhibitor AMG 510 drives anti-tumour immunity. Nature. 2019;575(7781):217-23.
14. Hong DS, Fakih MG, Strickler JH, Desai J, Durm GA, Shapiro GI, et al. KRAS(G12C) Inhibition with Sotorasib in Advanced Solid Tumors. N Engl J Med. 2020;383(13):1207-17.
15. Liu J, Kang R, Tang D. The KRAS-G12C inhibitor: activity and resistance. Cancer Gene Ther. 2022;29(7):875-8.
16. Awad MM, Liu S, Rybkin, II, Arbour KC, Dilly J, Zhu VW, et al. Acquired Resistance to KRAS(G12C) Inhibition in Cancer. N Engl J Med. 2021;384(25):2382-93.
17. Tanaka N, Lin JJ, Li C, Ryan MB, Zhang J, Kiedrowski LA, et al. Clinical Acquired Resistance to KRAS(G12C) Inhibition through a Novel KRAS Switch-II Pocket Mutation and Polyclonal Alterations Converging on RAS-MAPK Reactivation. Cancer Discov. 2021;11(8):1913-22.
18. Xue JY, Zhao Y, Aronowitz J, Mai TT, Vides A, Qeriqi B, et al. Rapid non-uniform adaptation to conformation-specific KRAS(G12C) inhibition. Nature. 2020;577(7790):421-5.
19. Tsai YS, Woodcock MG, Azam SH, Thorne LB, Kanchi KL, Parker JS, et al. Rapid idiosyncratic mechanisms of clinical resistance to KRAS G12C inhibition. J Clin Invest. 2022;132(4).
20. Ryan MB, Fece de la Cruz F, Phat S, Myers DT, Wong E, Shahzade HA, et al. Vertical Pathway Inhibition Overcomes Adaptive Feedback Resistance to KRAS(G12C) Inhibition.

Clin Cancer Res. 2020;26(7):1633-43.

21. Briscoe J, Therond PP. The mechanisms of Hedgehog signalling and its roles in development and disease. Nat Rev Mol Cell Biol. 2013;14(7):416-29.
22. Bangs F, Anderson KV. Primary Cilia and Mammalian Hedgehog Signaling. Cold Spring Harb Perspect Biol. 2017;9(5).
23. Garcia G, 3rd, Raleigh DR, Reiter JF. How the Ciliary Membrane Is Organized Inside-Out to Communicate Outside-In. Curr Biol. 2018;28(8):R421-R34.
24. Kong JH, Siebold C, Rohatgi R. Biochemical mechanisms of vertebrate hedgehog signaling. Development. 2019;146(10).
25. Huang P, Zheng S, Wierbowski BM, Kim Y, Nedelcu D, Aravena L, et al. Structural Basis of Smoothened Activation in Hedgehog Signaling. Cell. 2018;175(1):295-7.
26. Sasaki H, Hui C, Nakafuku M, Kondoh H. A binding site for Gli proteins is essential for HNF-3beta floor plate enhancer activity in transgenics and can respond to Shh in vitro. Development. 1997;124(7):1313-22.
27. Caspary T, Larkins CE, Anderson KV. The graded response to Sonic Hedgehog depends on cilia architecture. Dev Cell. 2007;12(5):767-78.
28. Dobin A, Davis CA, Schlesinger F, Drenkow J, Zaleski C, Jha S, et al. STAR: ultrafast universal RNA-seq aligner. Bioinformatics. 2013;29(1):15-21.
29. Love MI, Huber W, Anders S. Moderated estimation of fold change and dispersion for RNA-seq data with DESeq2. Genome Biol. 2014;15(12):550.
30. Duman-Scheel M, Weng L, Xin S, Du W. Hedgehog regulates cell growth and proliferation by inducing Cyclin D and Cyclin E. Nature. 2002;417(6886):299-304.
31. Katoh Y, Katoh M. Hedgehog target genes: mechanisms of carcinogenesis induced by aberrant hedgehog signaling activation. Curr Mol Med. 2009;9(7):873-86.

32. Jacob L, Lum L. Deconstructing the hedgehog pathway in development and disease. Science. 2007;318(5847):66-8.

33. Ruiz i Altaba A, Nguyen V, Palma V. The emergent design of the neural tube: prepattern, SHH morphogen and GLI code. Curr Opin Genet Dev. 2003;13(5):513-21.

34. Pugacheva EN, Jablonski SA, Hartman TR, Henske EP, Golemis EA. HEF1-dependent Aurora A activation induces disassembly of the primary cilium. Cell. 2007;129(7):1351-63.

35. Goldenson B, Crispino JD. The aurora kinases in cell cycle and leukemia. Oncogene. 2015;34(5):537-45.

36. Gupta S, Takebe N, Lorusso P. Targeting the Hedgehog pathway in cancer. Ther Adv Med Oncol. 2010;2(4):237-50.

37. Dai P, Akimaru H, Tanaka Y, Maekawa T, Nakafuku M, Ishii S. Sonic Hedgehog-induced activation of the Gli1 promoter is mediated by GLI3. J Biol Chem. 1999;274(12):8143-52.

38. Ikram MS, Neill GW, Regl G, Eichberger T, Frischauf AM, Aberger F, et al. GLI2 is expressed in normal human epidermis and BCC and induces GLI1 expression by binding to its promoter. J Invest Dermatol. 2004;122(6):1503-9.

39. Winklmayr M, Schmid C, Laner-Plamberger S, Kaser A, Aberger F, Eichberger T, et al. Non-consensus GLI binding sites in Hedgehog target gene regulation. BMC Mol Biol. 2010;11:2.

40. Peterson KA, Nishi Y, Ma W, Vedenko A, Shokri L, Zhang X, et al. Neural-specific Sox2 input and differential Gli-binding affinity provide context and positional information in Shh-directed neural patterning. Genes Dev. 2012;26:2802–2816.

41. Pandolfi S, Montagnani V, Lapucci A, Stecca B. HEDGEHOG/GLI-E2F1 axis modulates iASPP expression and function and regulates melanoma cell growth. Cell Death Differ.

2015:22:2006–201942. Rohatgi R, Milenkovic L, Scott MP. Patched1 regulates hedgehog signaling at the primary cilium. Science. 2007;317(5836):372-6.

43. Jia J, Tong C, Wang B, Luo L, Jiang J. Hedgehog signalling activity of Smoothened requires phosphorylation by protein kinase A and casein kinase I. Nature. 2004;432(7020):1045-50.
44. Zheng X, Mann RK, Sever N, Beachy PA. Genetic and biochemical definition of the Hedgehog receptor. Genes Dev. 2010;24(1):57-71.
45. Jiang J, Hui CC. Hedgehog signaling in development and cancer. Dev Cell. 2008;15(6):801-12.
46. Dennler S, Andre J, Alexaki I, Li A, Magnaldo T, ten Dijke P, et al. Induction of sonic hedgehog mediators by transforming growth factor-beta: Smad3-dependent activation of Gli2 and Gli1 expression in vitro and in vivo. Cancer Res. 2007;67(14):6981-6.
47. Nolan-Stevaux O, Lau J, Truitt ML, Chu GC, Hebrok M, Fernandez-Zapico ME, et al. GLI1 is regulated through Smoothened-independent mechanisms in neoplastic pancreatic ducts and mediates PDAC cell survival and transformation. Genes Dev. 2009;23(1):24-36.
48. Pietrobono S, Gagliardi S, Stecca B. Non-canonical Hedgehog Signaling Pathway in Cancer: Activation of GLI Transcription Factors Beyond Smoothened. Front Genet. 2019;10:556.
49. Huangfu D, Liu A, Rakeman AS, Murcia NS, Niswander L, Anderson KV. Hedgehog signalling in the mouse requires intraflagellar transport proteins. Nature. 2003;426(6962):83-7.
50. Tucker RW, Pardee AB, Fujiwara K. Centriole ciliation is related to quiescence and DNA synthesis in 3T3 cells. Cell. 1979;17(3):527-35.
51. Sanchez I, Dynlacht BD. Cilium assembly and disassembly. Nat Cell Biol.

2016;18(7):711-7.

52. Dummer R, Guminski A, Gutzmer R, Dirix L, Lewis KD, Combemale P, et al. The 12-month analysis from Basal Cell Carcinoma Outcomes with LDE225 Treatment (BOLT): A phase II, randomized, double-blind study of sonidegib in patients with advanced basal cell carcinoma. J Am Acad Dermatol. 2016;75(1):113-25 e5.
53. Sekulic A, Migden MR, Oro AE, Dirix L, Lewis KD, Hainsworth JD, et al. Efficacy and safety of vismodegib in advanced basal-cell carcinoma. N Engl J Med. 2012;366(23):2171-9.